chemosensors

MDPI

*Review*

# Hybrid Nanocomposites of Plasmonic Metal Nanostructures and 2D Nanomaterials for Improved Colorimetric Detection

**Caterina Serafinelli [1,2,3,4], Alessandro Fantoni [1,3,*], Elisabete C. B. A. Alegria [1,2] and Manuela Vieira [1,3,4]**

1 ISEL-Instituto Politécnico de Lisboa, 1949-014 Lisboa, Portugal; c.serafinelli@campus.fct.unl.pt (C.S.); ebastos@deq.isel.ipl.pt (E.C.B.A.A.); mv@isel.ipl.pt (M.V.)
2 Centro de Química Estrutural, Institute of Molecular Sciences, IST, Universidade de Lisboa, 1049-001 Lisboa, Portugal
3 CTS-Centre of Technology and Systems, 2829-516 Caparica, Portugal
4 DEE-FCT-UNL, Department of Electrotechnical, Computer Engineering of the Faculty of Science, Technology of the Universidade NOVA de Lisboa, 2829-516 Caparica, Portugal
* Correspondence: afantoni@deetc.isel.ipl.pt

**Abstract:** Plasmonic phenomena and materials have been extensively investigated for a long time and gained popularity in the last few years, finding in the design of the biosensors platforms promising applications offering devices with excellent performances. Hybrid systems composed of graphene, or other 2D materials, and plasmonic metal nanostructures present extraordinary optical properties originated from the synergic connection between plasmonic optical effects and the unusual physicochemical properties of 2D materials, thus improving their application in a broad range of fields. In this work, firstly, an overview of the structures and properties of 2D nanomaterials will be provided along with the physics of surface plasmon resonance and localized surface plasmon resonance. In the second part of the work, some examples of colorimetric biosensors exploiting the outstanding properties of hybrids nanocomposites will be presented. Finally, concluding perspectives on the actual status, challenges, and future directions in plasmonic sensing biosensing will be provided. Special emphasis will be given to how this technology can be used to support digitalization and virtualization in pandemic handling.

**Keywords:** 2D nanomaterials; metal nanoparticles; hybrid nanocomposites; plasmonic sensing



**Citation:** Serafinelli, C.; Fantoni, A.; Alegria, E.C.B.A.; Vieira, M. Hybrid Nanocomposites of Plasmonic Metal Nanostructures and 2D Nanomaterials for Improved Colorimetric Detection. *Chemosensors* **2022**, *10*, 237. https://doi.org/10.3390/chemosensors10070237

Academic Editors: Iole Venditti, Paolo Prosposito and Alessandra Paladini

Received: 29 April 2022
Accepted: 19 June 2022
Published: 22 June 2022



## 1. Introduction

During last few years, particularly from the outbreak of the coronavirus disease pandemic in 2019 (COVID-19) caused by a novel coronavirus, SARS-CoV-2 [1], the demand for cost-efficient, low consumption of reagents, ease of use, fast and sensitive biosensors to be applied in biomedical sectors and clinical treatment has exponentially increased. On this basis, the necessity of developing point-of-care (PoC) devices–sensing systems providing immediate results at any time and in any place, given the opportunity of customized care such that health outcomes will be improved—is more and more pressing. So, extensive research has been focused on biosensing, with growing interest toward plasmonics, namely the study of the interaction of electromagnetic radiation with electrons in solids. The blossoming of plasmonic biosensing has aroused the need of collecting the signs of progress achieved in the publication of reviews focused on critical discussions on its applications on PoC. In the work of Soler [2], the incorporation of plasmonic platforms into portable devices by means of nanotechnology, and the integration in today's devices, such as smartphones, along with the main challenges and limitations, have been discussed, while Salazar [3] identified four major areas of advances in plasmonic biosensing. The main one is related to the already well-established process that exploits local dimensional SPR (LSPR), while the other three areas are not yet consolidated and involve the use of different properties of the plasmonic system), whereas the other three areas are not consolidated yet and involve the

use of different properties of a plasmonic system. Thus, the chiral plasmonic properties, relevant for biological systems, the magneto-optical effects with tailored film architectures and quantum concepts to overcome the shot-noise limit in sensing and biosensing have been examined, and within these areas, the recent advances, challenges, and opportunities to exploit plasmonic platforms as an integral part of PoC devices have been discussed. In the work of Han [4], propagating plasmonic resonance mode based on planar design, plasmonic materials, and hybrid sensing techniques are exclusively reviewed for designs containing nanovoids in thin films, considering the notable potential offered by this type of plasmonic biosensors to be integrated into lab-on-a-chip devices. After reviewing the fundamentals of plasmonics allowing the development of an advanced biosensor, in the work of Liu [5], the materials and structures exploited as transducers for the analyte binding events into an optical signal (with a special focus on metal structures and graphene) have been considered along with their applications in real-life conditions examining the potential and the limitations. Stimulated by the development of a large number of novel materials, enormous progress has been made in plasmonic biosensors technology [6–8]. Novel materials have been exploited in a wide range of biosensing applications, but among these assays, colorimetric detection has driven growing interest related to its advantages: sophisticated or expensive instrumentation is not required because the color changes can be read by naked eyes, so they are characterized by simplicity, practicality and low cost [9]. The key issue in colorimetric detection is to convert the event of detection into a color change so that several smart materials, such as metal noble nanoparticles, magnetic and cerium oxide nanoparticles, graphene oxide, and carbon nanotubes have been developed to be exploited as platform sensing in colorimetric assays [10–13]. Recently, bidimensional (2D)-layered materials such as metal chalcogenides, transition metal oxides, and other 2D compounds have gained renewed interest due to their unique properties; nevertheless, their features have been further improved by integrating 2D material with plasmonic metal nanoparticles, thus generating outstanding structures. Inspired by the achievements reached in developing hybrids materials composed of 2D materials and plasmonic nanoparticles and by their enhanced optical and optoelectronics properties, Sriram, in his work [14], discussed the state-of-the-art of the hybrid device applications, such as Surface-Enhanced Raman Spectroscopy (SERS) analysis, hydrogen evolution reactions (HER) and photodetection, but the use of the hybrid systems in colorimetric detection has not been considered. In the same way, in the work of Li [15], the properties of the hybrid nanostructures have been discussed along with their use in photoelectronic applications to develop photovoltaic cells and photodetectors as well as their use in photocatalytic reactions such as photodegradation and hydrogen production and applications exploiting the optical signals such as SERS, photoluminescence (PL), and SPR sensors, but their applications in colorimetric detection have not been explored. Although the outstanding properties stimulated an increasing interest in research, along with the requirement of collecting the accomplished progress in the publication of reviews discussing their applications, there is still a lack of a critical review examining the use of hybrid compounds in colorimetric detection. Recent progress in the development, production, and applications of advanced biosensors based on 2D nanomaterials such as graphene, graphene oxide, transition metal oxide, MXene (compounds with a general formula Mn + 1XnTx, where M indicates the early d-transition metal atom, X indicates the N and/or C atom, and T means the surface terminated functional group, such as –OH, O and –F) and others have been discussed in the work of Zhu [16], but the physical and optical properties from which the outstanding characteristics of hybrid compounds arise are not reviewed. With the aim of fulfilling the gap in this direction and to help the research in developing more advanced detection systems, in the present work, the use of the hybrid metal nanoparticles/2D materials in the design and development of colorimetric assays will be reviewed, and a critical discussion on their future perspectives will be presented. It is necessary to appreciate the fundamental characteristics of the hybrid separate components, namely the plasmonic metal nanoparticles and the 2D nanomaterials, to examine the optical properties of the hybrid compounds, so that, firstly,

the plasmonic effect originated from metal nanostructures will be discussed in Section 2, along with the diverse physiochemical properties of 2D nanomaterials in Section 3. For a better understanding, attention is addressed to the basic principles of colorimetric detection in Section 4. In Section 5, the general properties of the metal/2D nanomaterial hybrids will be mentioned as well as their catalytic activity. After reviewing the properties of the hybrid structure, the exploitation of the colorimetric detection based on their peroxidase-like activity and reduction reaction and LSPR shifts will be considered in Section 6. Finally, in Sections 7 and 8, the future perspectives and conclusions will be critically addressed.

## 2. Optical Properties of Plasmonic Metal Nanoparticles

### *2.1. Physics and Working Principles of Plasmon Resonance*

The interaction of the electromagnetic field with an interface can generate appealing surface excitations. When the free electrons of a metal are coupled in resonance with the electromagnetic field of the radiation, surface-bound EM modes can be originated that are called surface plasmons (SPs). Usually, SPs are originated at the interface between a noble metal and a dielectric, thus satisfying the condition for the SPs excitation that requires two materials with optical constants of opposite signs connecting each other [17]. Often, SPs are classified in two categories: propagating surface plasmons (PSPs) and localized surface plasmons (LSPs) [18]. The physics and working principles behind the two classes of SPs will be revisited.

### *2.2. Propagating Surface Plasmon Resonances (PSPR)*

The first type of surface plasmon consists of running surface waves called propagating surface plasmons (PSPs): when a p-polarized light (radiation with its electric vector parallel to the plane of incidence, namely the plane perpendicular to the surface containing the incident and reflected wavevectors [19]) interacts with a metal surface, the free electrons in the metal react collectively, starting to oscillate in resonance with the light wave and propagate along the interface between metal nanostructures and dielectrics [20]. In this context, SPPs can be considered as light waves entrapped on the conducting material surface. The magnetic vector of PSPs is parallel to the plane of the interface and perpendicular to the direction of propagation of the wave, so that they can be referred as a transverse-magnetic (TM) polarized mode [21]. Because of their combined character between electromagnetic wave and surface charge, the SPWs should be termed surface plasmon polaritons (SPPs) to reflect the hybrid nature. As a consequence of the hybrid nature and in contrast to the propagating nature of PSPs along the surface, the EM field component perpendicular to the surface is maximum near the metal surface and decays exponentially at growing distances from it [22], so that in the dielectric medium at the top of the metal, the decay length of the field, $\delta_d$, is of the order of half the wavelength of light involved, whereas the decay length into the metal, $d_m$, is determined by the skin depth (Figure 1A). This means that most of the EM field is concentrated in the dielectric medium close to the metal surface, showing a typical penetration depth $\delta_d$ between 50 and 500 nm when working in visible or near-infrared (NIR) wavelengths. As a result, only the changes in refractive index occurring within the evanescent field are able to modify the SPP propagation and be detected, and this is relevant for SPRs analysis in view of the fact that biorecognition events taking place on the metal surface can be detected by exploring certain properties of the reflected light, such as angle, intensity or wavelengths. When the light vector is coupled to the surface plasmon such that the component of the light wavevector parallel to the interface matches the propagation vector of the SPP, the excitation of SPPs is reached, which is followed by a sharp dip in reflectance [20]. The dependence of the propagation vector on the refractive index of the dielectric is expressed by the SP dispersion relation [21], namely

the frequency-dependent SP wavevector calculated by solving the Maxwell equation with appropriate boundary conditions, thus obtaining:

$$k_x^{SPP} = \frac{\omega}{c}\sqrt{\frac{\varepsilon_2(\omega)\varepsilon_d}{\varepsilon_2(\omega)+\varepsilon_d}} \quad (1)$$

where $K_x{}^{SPP}$ is the wavevector component of SPP propagation, and $\varepsilon_d$ is the dielectric constant of the medium, which is directly related to the refractive index of the materials by the equation

$$\varepsilon_d = n^2 \quad (2)$$

$\varepsilon(\omega)$ is complex dielectric function of the metal depending on the frequency

$$\varepsilon(\omega) = \varepsilon_1(\omega) + i\varepsilon_2(\omega) \quad (3)$$

and $\omega$ and $c$ are the angular frequency and the speed of light in a vacuum, respectively. Observing the dispersion curve (Figure 1B), the excitation of surface plasmon polaritons can be explored: the SP mode always lies beyond the light line, that is, it has greater momentum ($\hbar k_{SP}$) than a free space photon ($\hbar k_0$) of the same frequency $\omega$ [22]. In this condition, the incident light cannot easily excite the surface plasmon polaritons: in order to achieve SPRs excitation, therefore, the resulting momentum mismatch between light and SPs of the same frequency must be overcome by enlarging the wavevector of the excitation light.

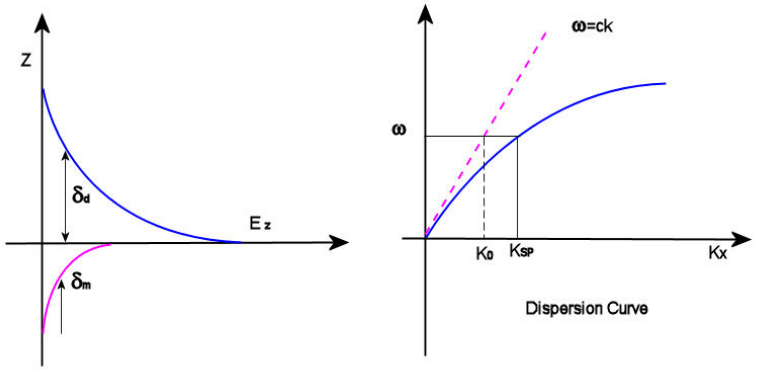


**Figure 1.** (**A**) $\delta_d$ (decay length of the field) and $\delta_m$ (decay length into the metal); (**B**) dispersion curve for an SP mode showing the momentum mismatch issue.

On this basis, the optical configurations for SPR analysis are classified according to SPP excitation method or the detection scheme [21]. The most common schemes are: (1) the *prism coupled Kretschmann* configuration, where an evanescent wave penetrating the metal film is generated by the light that is totally reflected at the base of a high refractive index glass prism when passing across it. The propagation vector of the evanescent wave can be adjusted by controlling the angle of incidence so that it mismatches that of SPPs; (2) the *grating couplers*, based on the light waves diffraction: in this case, the wavevector component of the diffracted light that is parallel to the interface is increased for a value inversely proportional to the period of the grating, so that can be matched with that of SPPs; (3) *waveguide structures*: when the light vector is coupled to the surface plasmon such that the component of the light wavevector parallel to the interface matches the propagation vector of the SPP, the excitation of SPPs is reached, which is followed by a sharp dip in reflectance. Due to the great potential of SPR analysis, much research has been performed in the last few years to develop enhanced SPR structures [23]; however, the use of hybrid plasmonic metal nanoparticles and 2D nanomaterials is only in its early stage. For the first time, a highly sensitive surface plasmon resonance (SPR) biosensor based on AuNPs/$MoS_2$ hybrid nanostructures for microRNA (miRNA) detection has been

presented by Nie et al. [24]. The sensing platform has been produced following a two-step protocol: in the first stage, the captured DNA consisting of a thiol-modified probe including a sequence complementary to the target miRNA has been immobilized on the Au film, and then, DNA-linked AuNPs/$MoS_2$ nanocomposites were used to combine with the other section of the miRNA-141, thus creating a sandwich structure. The sensing platform has been exploited in SPR analysis, detecting the resonance angle in the presence of a different concentration of miRNA-141. The so-developed sensing system displayed high sensitivity toward miRNA detection, where the improved performances originated from the presence of AuNPs/$MoS_2$ nanohybrids. The signal amplification of the structure has been assigned to three main causes: the first cause is the synergistic effect of LSPR of AuNPs on SPR waves, whereas the second one is a larger number of AuNPs in the system due to the presence of $MoS_2$ nanosheets and finally, SPR in AuNPs-$MoS_2$ nanocomposites could be actively controlled by the photoexcited excitons, resulting in an enhancement of SPR signal. As a consequence of the signal amplification due to the presence of the AuNPs/$MoS_2$ hybrids in the sensing system, the very lower limit of detection (LOD) of 0.5 fM has been reached. The additional advantages of the developed sensing platform are its high specificity, acceptable reproducibility, and precision; furthermore, the system is low-cost and enzyme-free. The SPR assay based on AuNPs/$MoS_2$ has been exploited also to detect human miRNA from cancer cells with excellent results, thus providing great potential for miRNA quantification in clinical diagnosis and disease treatment.

### *2.3. Localized Surface Plasmon Resonances (LSPR)*

The interaction of the light with subwavelength-sized metallic particles emerges in the non-propagating collective oscillations of the particle conduction electrons, which are named localized surface plasmon resonance (LSPR). As a result of the LSPR, there is an accumulation of charges on the particle surface functioning as a dipole. The presence of LSPR acting as an oscillating dipole in a nanoparticle is the basis of two phenomena. Firstly, the optical extinction of the particle reaches its maximum value at the frequency of plasmon resonance, taking place in the visible range for noble metal nanoparticles. Secondly, the electromagnetic fields localized close to the particle surface are largely enhanced, with the enhancement being higher at the surface and quickly decreasing when the distance becomes greater. In order to reach a deeper understanding on the LSPR origins, the scattering theory must be considered as well as the interactions between the spherical nanoparticle and the light discussed in view of Mie Theory [25]. In the famous paper published in 1908 [26], Gustav Mie illustrated a first overview on how to calculate the scattering and absorption of light by spherical particles, developing an analytical solution to Maxwell's equations. By means of his calculations, he was able to explain the color of gold colloids changing with the size of gold spheres, which was a phenomenon later interpreted considering surface plasmon resonances. When the diameter of metallic spherical nanoparticles is much smaller than the incident light wavelength ($Ø << \lambda$ where $Ø$ is the particle diameter and $\lambda$ is the incident light wavelength), the charge oscillations act as a single dipole whose amplitude is strongly dependent on the distances between the surface charges, whereas the external electromagnetic (EM) field in the close vicinity of the nanoparticle surface appears static. Under these conditions, Mie scattering agrees with the more familiar Rayleigh scattering. The condition of LSPR is related to the particle polarizability, $\alpha_0$, expressed by Equation (2) [27]:

$$\alpha = 4\pi R^3 \frac{\varepsilon(\omega) - \varepsilon d}{\varepsilon(\omega) + 2\varepsilon d} \quad (4)$$

Concerning plasmonic effects, polarizability is a crucial factor, since it describes the predisposition of the electronic cloud to have its charge displaced as a result of the interaction with an electrical field, so that it is related to the dipole moment **p** by the relation:

$$\mathbf{p} = \varepsilon_0 \varepsilon_d \alpha \mathbf{E_0} \quad (5)$$

From Equation (4), it is possible to observe that the polarizability $\alpha$ is dependent on the dielectric function of the metal $\varepsilon(\omega)$ expressed by Equation (3), where $\varepsilon_1(\omega)$ is the real part of the dielectric function and $\varepsilon_2(\omega)$ is the imaginary part. In addition, Equation (4) shows that the polarizability is dependent on the dielectric constant of the surrounding medium, which is related to the refractive index n of the medium by Equation (2). The condition for which the polarizability $\alpha$ achieves the resonant enhancement, namely its maximum value, is fulfilled at the minimum values of the denominator in Equation (2) (Frölich condition). For Equation (4), the Frölich condition at which LSPR occurs is satisfied for $\varepsilon_1(\omega) = -2\varepsilon_d$. On this basis, to determine an LSPR in a nanoparticle, the values of $\varepsilon 1(\omega)$ (the real part of the dielectric function) should be large and negative, whereas the imaginary part $\varepsilon 2(\omega)$ is supposed to be negligible and positive [28]. In the case of noble metals, the dielectric function $\varepsilon'_m$ is strongly dependent on the EM field wavelength, so the bright colors displayed by metal nanoparticles definitely rely on the exact wavelength fulfilling the condition of resonance. The most used metal for LSPR sensing satisfies the resonance condition in the UV-visible region of the spectra. The bandwidth and peak position of LSPR are determined by the size, morphology, and distance of separation between the nanostructures so that they can be easily tailored and tuned in the UV-visible and NIR region of the spectrum. However, LSPR strongly depends also on the dielectric constant of the medium around the metal nanoparticles, so that, according to the changes in refractive index (RI) of the medium within the evanescent field, the particle polarizability is modified, resulting in displacements of the LSPR peak. On this basis, the sensitivity toward the changes in refractive index is exploited to detect biorecognition events occurring on particle surface, thus offering a great potential to develop sensing platforms. In Figure 2, the LSPR of a plasmonic metal nanoparticle (Figure 2A) and the SPPs (Figure 2B) are depicted.

In addition, intense and highly confined electromagnetic fields generated by the LSPRs, and localized within the gaps between metallic nanostructures, are of great interest for other sensing techniques, such as SERS. In SERS analysis, the inelastic scattering generated by molecules is greatly boosted when molecules are located closed (or adsorbed) to a rough metal surface or metal nanoparticles, thus enhancing the signal. The history of SERS is relatively short, considering that it has been observed for the first time in the work of Fleischmann in 1974 [29] in the course of Raman measurements of pyridine adsorbed on an electrochemically roughened silver surface. In 1977, two groups, observing independently that the enhanced signal did not account for the concentration of scattering species, proposed two different mechanisms: the group of Albrecht and Creighton [30] proposed a charge-transfer effect, while D. L. Jeanmaire and Richard P. Van Duyne [31] proposed an electromagnetic effect. Since then, an exponentially growing interest has been focused on improving the SERS substrates to enhance the performance of the technique but also to implement these structures in the point-of-care (PoC) devices. In the last few years, hybrid compounds composed of bidimensional nanomaterial have been exploited with an increasing frequency as SERS substrate [32], but also, other types of composites have been exploited, such as for example metal–organic framework (MOF)–gold nanoparticle (AuNPs) complexes [33].

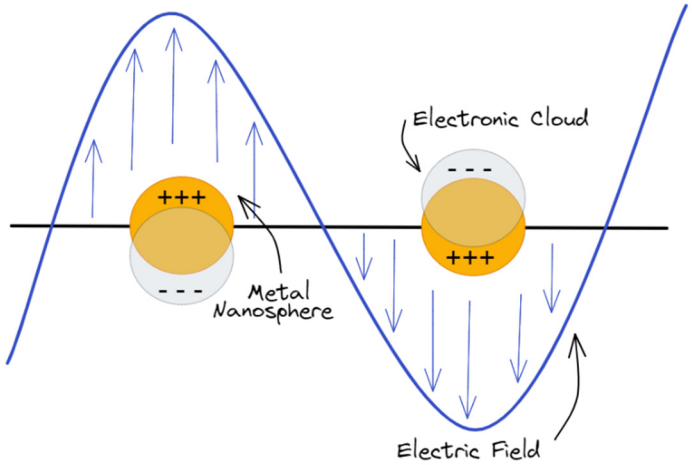


(**A**)

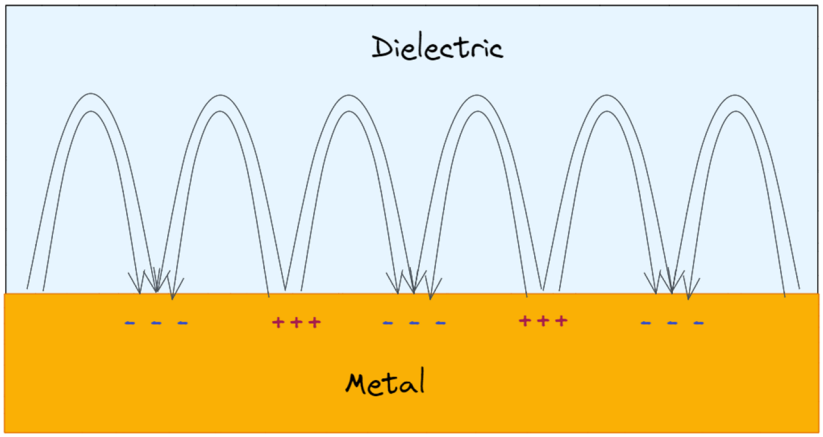


(**B**)

**Figure 2.** (**A**) Schematics of metal nanoparticles with their LSPR when placed in a static electromagnetic (EM) field; (**B**) collective charge oscillations (SPPs) at the interface between the dielectric medium and the metal.

## 3. Properties of 2D Nanomaterials

### *3.1. Transition Metal Dichalcogenides (TMDCs)*

Transition metal dichalcogenides (TMDCs) are a large family of materials of $MX_2$ type, where M is a transition metal element from group IV, V or VI and X is a chalcogen (S, Se or Te). They possess a layered structure, and each layer includes three atomic planes with an arrangement of X-M-X type, where a hexagonally packed plane of transition metal atoms M is enclosed within two atomic planes of chalcogen X, resulting in a thickness of 6–211 7 Å for every single layer [34]. The interactions between atoms within the same atomic plane are in their essence covalent, whereas the layers inside the structure are connected by Van der Waals forces. In Figure 3, a $WS_2$ monolayer is represented.

One of the intriguing properties of TMDCs is polymorphism [35]: when in their bulk form, three polymorphs are shown, namely the 1T, 2H and 3R, where the number indicates the number of atomic planes within the unit cell and the letter indicates the symmetry. In the 1T structural polytype, the symmetry is tetragonal, the coordination of the metal atom is octahedral, and one monolayer is present in each unit cell; in 2H, the symmetry is hexagonal, the coordination of the metal atom is trigonal prismatic, and there are two monolayers inside the cell unit; finally, in 3R polymorphs, three monolayers are found in each unit cells, the metal atom coordination is trigonal prismatic and the symmetry is rhombohedral. These different structural phases originated from the different stacking orders of the chalcogen–metal–chalcogen atomic planes, forming the single layer of TDMs.

In the 2H phase, the chalcogen atoms in different atomic planes are located in the same position A, so that one is located on the top of the other in a perpendicular direction of the layer. This configuration of atomic planes corresponds to a stacking of ABA type. On the other hand, the 1T phase is characterized by a stacking of ABC type. Combining different chalcogens with different transition metals, it is possible to obtain the 1T or 2H phases, but it is possible to achieve the other as a metastable phase [36]. The outstanding properties of TMDCs are strongly correlated to the number of layers forming the structure. When passing from the bulk state to the monolayer structure, several semiconducting TMDCs undergo a transition from an indirect bandgap to a direct bandgap such as in the case of molybdenum disulfide ($MoS_2$). $MoS_2$ is one of the most representative TMDCs. In its bulk form, $MoS_2$ is an indirect bandgap semiconductor with a bandgap of about 1.3 eV, but when exfoliated to a single-layer structure, it goes through a transition to the direct band semiconductor, with a bandgap of about 1.8–1.9 eV [37]. The transformation of electronic structure arising from the different number of layers in the $MoS_2$ structure can be perceived in their spectra of photoluminescence (PL). When in its bulk form, the PL emissions arising from $MoS_2$ are inappreciable, but upon reducing the number of layers forming the structure, the PL becomes more pronounced at ≈670 and ≈627 nm. The PL emissions are generated by the direct excitonic transitions at the Brillouin zone K point. In addition, it has been shown that when the number of layers is reduced, the PL intensity becomes stronger and the quantum efficiency is higher, with the monolayer displaying the best values [38]. The capability of an efficient fluorescence quenching for fluorophores displayed from TMDCs gave them great potential to be exploited in the implementation of fluorescence-based biosensors.

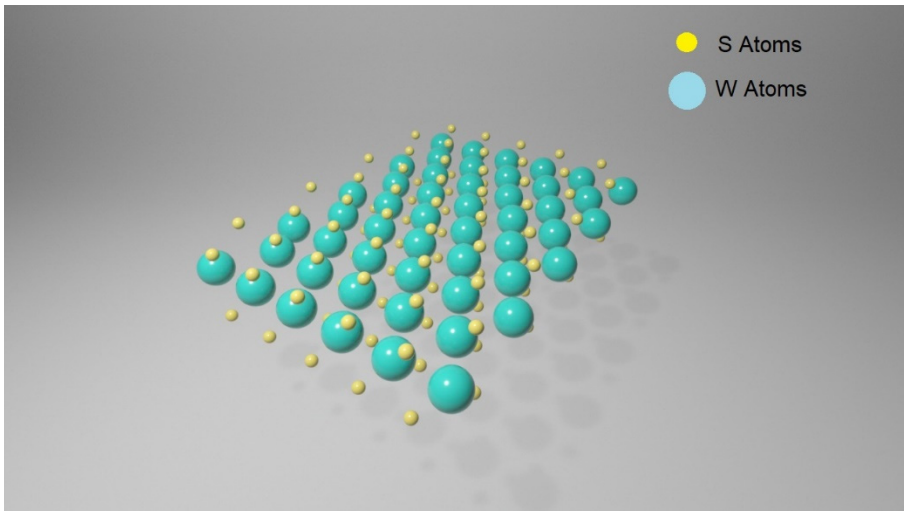


**Figure 3.** Schematic of a $WS_2$ monolayer: plane consisting of W atoms (in green) and S plane (in yellow).

### *3.2. Peroxidase-Like Activity*

Between TMDs compounds, $MoS_2$ and tungsten disulfide ($WS_2$) possess a peroxidase-like activity that makes their use as mimics of the enzyme possible. In his work, Guo [39] used for the first time $MoS_2$ nanosheets to catalyze the peroxidase substrate 3,3′,5,5′-tetramethylbenzidine (TMB) in the presence of $H_2O_2$. On the basis of these results, a colorimetric assay for the sensitive and selective detection of glucose in human blood has been developed. Because of the p-type nature of few-layer $MoS_2$ material, the electron can transfer from TMB to $MoS_2$ nanosheets: during this process, the TMB molecules are able to donate the lone-pair electrons from the amino groups to $MoS_2$ nanosheets on which they are adsorbed, such that the electron density and mobility in $MoS_2$ nanosheets are increased. As a result, the electron transfer from $MoS_2$ nanosheets to $H_2O_2$, producing the reduction of $H_2O_2$ to $H_2O$, is accelerated, thus increasing the rate of oxidation reaction of TMB by $H_2O_2$. In a successive work [40], Guo exploited the same process to develop a colorimetric

assay to detect glucose in human blood, but exploiting $WS_2$ nanosheets in place of $MoS_2$ nanosheets, thus confirming their peroxidase-like activity.

### *3.3. Catalytic Activity*

Chemically exfoliated $MoS_2$ nanosheets with a prevailing contribution of metallic 1T phase reveal a high catalytic activity comparable to that of many catalysts based on noble metals toward several models of reduction reactions performed in an aqueous environment at room temperature and employing $NaBH_4$ as the reducing agent [41]. Despite the good performances displayed in the metallic phase, $MoS_2$ in its trigonal prismatic (2H polymorph) is by nature a semiconductor, so its intrinsic conductivity is relatively low [42]; nevertheless, in order to perform a redox process, the electrons must be effectively exchanged between the catalytic active center and the reagent to improve the catalytic reaction kinetics. With the aim of promoting electron transfer, $MoS_2$ nanosheets have been integrated with 2D graphene or 3D conductive supports. Incorporating plasmonic nanoparticles onto the surface proved to be the most promising strategy to enhance the peroxidase-like activity of $MoS_2$ nanosheets [43].

## 4. Fundamental Principles of Colorimetric Analysis Based on Plasmonic Nanoparticles

The mechanism behind the colorimetric detection is dictated by the outstanding properties of the plasmonic nanoparticles, so, in this review, the colorimetric assays will be classified into two main categories on the basis of the property exploited to cause the color change. The first one is based on the LSPR shifts generated by the plasmonic properties of the particles, whereas the other one is based on their enzyme-mimic activities.

### *4.1. Colorimetric Sensors Based on SPR Change*

Taking into account that the absorbance (namely the color) is modulated by the shape/morphology, size, distribution, and metal composition, as well as the local environment in which the plasmonic nanoparticles are immersed and by the interparticle distance, in colorimetric sensing, the signal (i.e., the color change) can be originated by varying one of these parameters, resulting in a modification of their optical absorbance and in an LSPR shift in the UV-spectra. The first class of plasmonic biosensors considered in this work is the one based on color change generated by the LSPR shifts, and the different strategies at the basis will be considered. In line with different mechanisms designed to cause an LSPR shift, it is possible to find strategies based on the interparticle distance changes. Commonly, the mechanism causing the variation of the interparticle distance is the aggregation of metal plasmonic nanoparticle. According to the aggregation strategy, the plasmonic assay is based on the color change (associated to an LSPR change in the UV spectra) occurring when plasmonic nanoparticles swap in an aggregated state from the individual one by means of the selective action of the analytes. For this kind of assay, particles with a high cross-extinction section such as Au and Ag are the most appropriate, allowing also colorimetric assays based on detection by the naked eye [44]. Due to its advantages, such as fast response, free from bulky and expensive instrumentation, simplicity, sensitivity and portability, a lot of research has been focused on developing colorimetric assays based on aggregation of plasmonic metal nanoparticles. The pioneering work of Mirkin [45] paved the way to a new kind of sensing: in this study, firstly, AuNPs have been modified with thiolated DNA, and then, aggregation was generated by the reaction with the complementary DNA, resulting in a color change from red to blue, making it possible to observe the reaction by the naked eye. From this work, the approach has been exploited in different fields such as for example the detection of heavy ions, which is of interest in biological, environmental, and food safety applications. For example, in the work of Zhang [46], peptide-modified AuNPs have been successfully exploited for the parallel detection of $Cd^{2+}$, $Ni^{2+}$, and $Co^{2+}$ ions. In this case, the peptide-functionalized particle has been designed to have the ability to recognize and bind $Cd^{2+}$, $Ni^{2+}$ and $Co^{2+}$ over other metal ions, so that in the presence of such ions, the color of the solution turned from red to

blue. The color change is associated with the aggregation of the AuNPs, resulting from the binding between the peptide functionalizing the AuNPs surface and the metal ions. The prepared AuNPs displayed a peak at 520 nm in the UV spectra, and when adding $Cd^{2+}$, $Ni^{2+}$ and $Co^{2+}$ ions, the peak shifted to longer wavelengths due to the aggregation of the particles, so monitoring the absorbance ratio at 520 nm and 600 nm (A520/A600) allowed plotting the calibration curve for a detection limit as low as 0.05 µM $Cd^{2+}$, 0.3 µM $Ni^{2+}$ or 2 µM $Co^{2+}$. In the work of Wen [47], polyethyleneimine (PEI)-stabilized gold nanoparticles (PEI/AuNPs) have been synthesized and exploited for heparin detection. Heparin is a negatively charged polysaccharide used in clinical procedures as an anticoagulant, so that is able to create electrostatic interactions with the positively charged aminic groups of PEI functionalizing the AuNPs surface. As a result of the electrostatic interactions, the aggregation of AuNPs is induced, resulting in a color change. Colorimetric assays based on the aggregation of plasmonic metal nanoparticles offer a great potential for the fast and easy detection of analytes, so they have attracted great attention during the outbreak of coronavirus disease 2019 (COVID-19) caused by the severe acute respiratory syndrome-coronavirus-2 (SARS-CoV-2). To contain and downregulate the pandemic spreading, a rapid, handy, and large-scale diagnosis is requested, so many efforts have been focused on this direction [48]. Motivated by its characteristics, in the work of Moitra [49], a colorimetric assay for the selective naked-eye detection of SARS-CoV-2 has been developed. Gold nanoparticles have been synthesized, and their surfaces were functionalized with thiol-modified antisense oligonucleotides (ASOs) specific for N-gene (nucleocapsid phosphoprotein) of SARS-CoV-2: in presence of its target RNA sequence of SARS-CoV-2, the ASO-capped AuNPs aggregate, causing a shift in the LSPR spectra and observing a color change from violet to dark blue. As discussed in Section 2.3, in order for LSPR to occur, the dielectric function of the metal must be composed by a large and negative real $\varepsilon 1(\omega)$ and a small and positive imaginary part $\varepsilon 2(\omega)$, and while metals such as silver and gold fully satisfy these requirements, other metals such as for example copper fulfill that criterion in the same manner [50], but in contrast to Au and Ag, they are unstable and inclined to surface oxidation so that their optical properties are influenced and their handling is difficult. Because of its instability, the copper nanoparticles (CuNPs) remain unexplored for practical applications. Motivated by the lower cost compared to Au and Ag nanoparticles, Laghari in his work [51] used CuNPs as a sensing system, despite their challenging formation. In this work, CuNPs have been produced without the protection of inert gas and reducing the precursor with hydrazine in the presence of ranolazine acting as the capping agent (Rano-CuNPs). After the synthesis, the Rano-CuNPs have been tested for $As^{3+}$ ions detection: when adding $As^{3+}$ ions, the Rano-CuNPs solution turns from red brick to dark green, while in the UV spectra, the LSPR decreased in intensity and red-shifted. From the linear regression plot of the change in absorbance ($\Delta A$) versus $As^{3+}$ concentration, an LOD of $1.6 \times 10^{-8}$ M and from the comparison with the results obtained in the previous methods, the authors found that it was the lower. The redshift of the LSPR peak has been justified by the aggregation of Rano-CuNPs: in the presence of $As^{3+}$ ions, ranolazine is removed from the surface, thus destabilizing the nanoparticles and causing their aggregation. Different from assays based on aggregation, other strategies rely on the etching or growing of plasmonic metal nanoparticles: in this case, the shift of LSPR peak with the connected color change is originated from variations in the size and shape of plasmonic nanoparticles. For example, in the work of Guo [52], a colorimetric approach has been developed for the detection of molecules based on the enzyme-directed growth of silver nanoparticles (AgNPs) on the surface of gold nanostars (AuNSs). In this case, the strategy has been designed to detect alkaline phosphatase (ALP), which is an important biomarker in clinical diagnoses such as prostatic cancer, hepatitis, and bone disease. When ALP is added to a solution containing AuNSs, $Ag^{+}$ ions and ascorbic acid 2-phosphate (AAP), the ALP-catalyzed dephosphorylation of AAP takes place, producing ascorbic acid (AA). The so-formed AA then reduces the Ag+ in the solution to produce silver nanoparticles (AgNPs) on the AuNSs surface. As a result of the AgNPs formation on the AuNSs surface, the solution turns from blue to

dark blue, purple, and ultimately orange when the ALP concentration increased, whereas at the same time, the LSPR of AuNSs in the UV-spectra blue-shifted. Because the LSPR shift is dependent on the amount of ALP introduced into the system, a calibration curve has been created plotting the LSPR shift versus the logarithm of ALP concentration, from which an LOD of 0.5 pM has been calculated. Differently, other approaches are based on the etching of plasmonic metal nanoparticles. In the work of Xu [53], a colorimetric assay for glucose, based on enzymatic etching of gold bipyramids (AuNBPs), has been designed: from the horseradish peroxidase (HRP) catalyzed oxidation of glucose, peroxide hydrogen is formed that successively is broken into OH• radicals. The so-generated hydroxyl radicals (OH•) were able to etch the AuNBPs, causing a blue-shift of the LSPR peak, from which the glucose is detected. Although colorimetric assays performed in solution offer great potential for a fast, sensitive and easy detection of molecules, special attention must be paid to the stability of plasmonic metal nanomaterial, since unexpected aggregation can be induced by changing the environmental conditions such as buffer composition, pH, salts concentration, etc., so that false negative or positive signals can occur, invalidating the detection results. To avoid the issues correlated to the assays in solution, in other strategies, the plasmonic metal nanoparticles are deposited on the surface of a substrate: under these circumstances, the LSPR is generated by the change in the dielectric around the particle surface. The most common approaches used a glass slide as a substrate [54], but other substrates are attracting growing attention for their intrinsic properties, such as for example in the work of Shiohara [55], where a monolayer of gold nanostars (AuNSs) has been uniformly deposited with a high density on a polydimethylsiloxane (PDMS) and tested as an LSPR sensing platform. The choice of PDMS was motivated by its properties: PDMS is an optically transparent elastomer, inert, non-toxic, non-flammable, and flexible. Because of its flexibility, PDMS substrates could be wrapped around a non-flat surface for detection. Using the model analyte mercaptoundecanoic acid for analysis based on the LSPR shifts originating from refractive index changes, the sensing platform displayed good results, thus showing a great potential for LSPR sensing. In the work of Tadepalli [56], gold nanorods (AuNRs) functionalized with appropriate biorecognition elements (BRE) have been deposited on a regular laboratory filter paper and successfully tested for the cardiac biomarker troponin I (cTnI) detection. The created bioplasmonic paper device (BPD) offers a great potential for use in resource-limited settings, because it does not require special storage conditions.

### *4.2. Colorimetric Detection Based on Catalysis by Enzyme-Mimic Nanomaterials*

Whereas in the first group, the color change originated from an LSPR shift resulting from the different shape, size, or dielectric environment of the plasmonic nanoparticle induced by the analyte, in the second group of biosensors, the detection of molecules is based on the peroxidase-like activity of the plasmonic nanoparticles. Natural enzymes are able to catalyze organic reactions, but despite their intriguing potential in colorimetric detection, they display some drawbacks: they are not stable, thus becoming easily denatured, could lose their activity when purified, stored, or applied, and are expensive, so that in the last few years, an increasing interest in developing them has been focused on designing and developing nanomaterials with enzyme-mimic characteristics aiming to overcome the critical characteristics of the natural enzymes [57]. Among the natural enzymes, horseradish peroxidase (HRP) has received great attention for its ability to catalyze the oxidation of a dye resulting in a color change generated by the formation of the product, such that a broad variety of peroxidase mimic nanomaterials have been designed and developed for colorimetric detection. Usually, the catalytic activity of peroxidase is evaluated by peroxidase substrates such as 3,3′,5,5′-tetramethylbenzidine (TMB), diazoaminobenzene (DAB), o-phenylenediamine (OPD) and 2,2′-azino-bis(3-ethylbenzothiazoline-6-sulfonic acid) (ABTS): when they are oxidized by peroxidase in the presence of hydrogen peroxide ($H_2O_2$), a color change is generated by the formation of the product [58]. Metal plasmonic nanoparticles have attracted great interest in catalysis because, in addition to their out-

standing optical and physical properties, they show a high surface-to-volume ratio. While the plasmonic properties of Au and Ag nanoparticles have been extensively exploited for colorimetric sensing, fewer efforts have been invested in a deep insightful understanding of the optical properties of other metals such as Pd nanoparticles (PdNPs). However, in the last few years, some works focused on a critical review of the plasmonic behavior of PdNPs, with the aim to facilitate their future applications in advanced devices. In the work of Sugawa [59], the extinction spectra of Pd nanospheres (PdNSs) surrounded by water ($n$ = 1.33) and with a diameter (d) comprised in the range 10–200 nm, and from the calculated extinction spectra, it is possible to note that for a particle with d < 40 nm, the LSPR is localized in the region of the spectra with wavelengths lower than 200 nm, whereas particles with diameters between 50 and 90 nm display a dipolar LSPR in the near ultraviolet region. For particles with a diameter larger than 90 nm, the optical response broadens because, along with dipolar modes, higher-order modes start to appear. In addition, the factors at the basis of the refractive index sensitivity of plasmonic PdNPs have been examined. On the basis of the Frölich condition, the wavelength at which the LSPR takes place depends exclusively on the relation between the real part of the metal-dielectric function ($\varepsilon 1(\omega)$) and the surrounding medium ($\varepsilon$m); since the value of $\varepsilon 1(\omega)$ relies on the wavelength λ (namely, each λ corresponds a different value of $\varepsilon 1$), the LSPR frequency is strictly related to how the dielectric function change with the wavelength. Considering the dependence of $\varepsilon$m on the refractive index of the medium n (eq), in the plot of $\varepsilon 1$ versus the wavelength λ, the range of λ at which the LSPR occurs for the values of n comprised between 1.333 and 1.440 has been highlighted, and it has possible to observe that Pd controls the broadest resonance wavelength range: it means that for changes in the refractive index, Pd shows the larger LSPR shifts. The theoretical and experimental sensitivity of PdNPs toward the refractive index changes has been calculated and compared with that of AuNPs and AgNPs, showing the higher sensitivity of PdNPs. Successively, the plasmonic properties of PdNPs have been critically reviewed in the work of De Marchi [60]. In this work, the real part $\varepsilon 1(\omega)$ of the dielectric function has been related to the angular momentum l (establishing the order of the resonance mode for spherical particles) and the factor shape Li for anisotropic ellipsoidal particles, so that, from the plot of $\varepsilon 1$ for Au, Ag and Pd versus λ, it is possible to observe that $\varepsilon 1$ changes more slowly in the case of Pd compared to Au and Ag; that is, the slope of the curve is lower for Pd. The lower value of the slope results in a broader range of wavelengths at which LSPR takes place when the particle shape changes, thus indicating the higher sensitivity of PdNPs to shape variations. In the work of Langhammer [61], the large sensitivity toward the change in size has been demonstrated for Pd nanodisks. Small Pd nanodisks with a height of 20 nm and a diameter of 38 nm display an LSPR peak at 200 nm, whereas nanodisks with the same size but made of Ag display an LSPR peak centered at 500 nm. Larger Pd nanodisks with a height of 20 nm and a diameter of 530 nm show an LSPR at 1800 nm, whereas for nanodisks made of Ag with the same size, the LSPR peak is centered at 1600. It means that in case of PdNPs, when the size changes, there is a shift from 200 to 1800 nm, a range of 1600 nm, whereas in the case of AgNPs, there is a shift of 1100 nm (from 500 to 1600 nm), thus showing the higher sensitivity of PdNPs to change in shape compared to AgNPs. From the absorbance properties of PdNPs arises the necessity of designing synthetic routes to fabricate Pd nanoparticles with well-defined optical features, so that, despite the potential to become the third plasmonic sensing material, its use in colorimetric detection based on LSPR shifts remains unexplored, and in this work, we will consider the use of PdNPs in colorimetric assays only on the basis of their enzyme-mimic activity. In the work of Rastogi [62], Pd nanoparticles have been synthesized in a simple single-step green method, using the gum kondagogu (GK) as the reducing and capping agent. In the presence of TMB and $H_2O_2$, the so-obtained Pd nanoparticles (GK-Pd NPs) displayed a good peroxidase-like activity, thus showing the potential for the colorimetric detection of cholesterol. The oxidation of cholesterol catalyzed by cholesterol oxidase (ChOx) produces 4-cholesten-3-one and $H_2O_2$, and the peroxide hydrogen formed in the presence of GK-Pd NPs reduces the TMB molecules in the system so that the peak at

652 nm of the reduced TMB starts to appear in the UV-visible spectra. At the same time, the color of the solution turns into blue from dark brown. For the growing concentration of cholesterol, the absorbance of the peak at 652 nm increased, so by the calibration curve of the absorbance at 652 nm versus cholesterol concentration, a limit of quantification of 3.7 μM has been found. In the work of Jin [63], small Pt nanoclusters (Pt NCs) have been synthesized and exploited for glucose detection. Small PtNCs with an average size of about 3 nm have been produced using yeast extract acting as the reducing agent of the precursor and the stabilizer of the particles, and their peroxidase-like activity was tested: in the presence of PtNCs, the oxidation of TMB by $H_2O_2$ takes place, producing a color change from colorless to blue, and a peak centered at 652 nm starts to appear in the UV-spectra. In the absence of PtNCs or $H_2O_2$, the system remained colorless, and no peak is observed in the UV spectra, confirming that both PtNCs and $H_2O_2$ are required and PtNCs is able to catalyze the oxidation of TMB, confirming its peroxidase-like activity. Taking advantage of the peroxidase-like activity, in the same work, a rapid colorimetric biosensor for glucose has been developed. Glucose is oxidized by means of the reaction with $O_2$ catalyzed by glucose oxidase (GOD), producing $H_2O_2$ and gluconic acid. The $H_2O_2$ produced by the reaction of oxidation successively reacts with the TMB molecules present in the system so that a colorimetric reaction of TMB reduction occurs and was used as a colorimetric assay. In this work, the nature of peroxidase-like activity of PtNPs has been assigned to its ability to facilitate the electron transfer between TMB and $H_2O_2$. For the PtNCs-catalyzed reduction of TMB with $H_2O_2$, it has been found that a Langmuir–Hinshelwood mechanism gives a better description of the kinetic data [64]. According to the proposed mechanism, in the first step, TMB and peroxide hydrogen molecules are adsorbed on the particle surface and are decomposed, thus generating surface-bound reactive oxygen species (ROS). Successively, the so-produced ROS can react with the adsorbed TMB molecules in the step, determining the rate of the reaction, and the formed product is desorbed from the surface. Asides from their peroxidase-like activity, metal nanoclusters display a reductive activity, and usually, the catalytic reduction of 4-nitrophenol (4-NP) to 4-aminophenol (4-AP) is employed as a model reaction to evaluate the catalytic performances of AuNPs. Wunder et al. [65] proposed the Langmuir–Hinshelwood mechanism as a model for the reduction of 4-NP by $NaBH_4$ in the presence of metallic nanoparticles. According to the proposed mechanism, the surface of metal nanoparticles is the place where the process of the catalytic reduction takes place: borohydride ions as well as 4-NP molecules adsorb on the metal nanoparticle surface, so that borohydride ions reduce 4-NP molecules, becoming the step determining the rate of the reduction. In this contest, the surface of the particle is a critical factor: during the catalytic process, ligands are displaced by the substrates, so that no induction time is observed when ligands are easily removed, whereas longer induction times are observed for strongly adsorbed ligands. In view of that, several strategies are focused on facilitating the displacement process between the ligands and substrates on the surface to increase the rate constants and the catalytic activity of the metal nanoparticles. The reduction of 4-NP catalyzed by metal nanoparticles is also used as a colorimetric-sensing strategy. For example, a colorimetric assay for cocaine detection based on the catalytic activity of the AuNPs surface toward the reduction of 4-NP has been developed in the work of Abnous [66]. In this case, the formation of a triple-fragment aptamer (TFA) on the AuNPs surface is induced by the presence of cocaine, resulting in a substantial reduction of the AuNPs catalytic activity so that the solution remains yellow. When there is no cocaine, TFA is not formed, so that 4-NP can easily bind to the particle surface, facilitating its reduction and, as a result, the solution turns from yellow to colorless, indicating the formation of the product, the 4-AP. From the calibration plot, an LOD of 440 pM has been found. In addition, the colorimetric assay has been tested for cocaine detection in spiked human serum samples obtaining good results, thus showing great potential in clinical diagnosis.

## 5. Properties of Hybrids Compounds

### *5.1. General Properties*

Despite the exceptional properties displayed by 2D nanomaterials, they reveal some drawbacks; the most challenging of them is the interaction of the light with the materials, resulting in lower light absorption and emission caused by the thickness at atomic scale [67], so they cannot be efficaciously exploited in all applications, especially for light-driven ones. With the intention to address the needs of the practical applications, increasing the light absorption of 2D nanomaterials has become a critical point. The most promising strategy developed in the last few years, which is attracting growing interest, consists of integrating 2D nanomaterials with plasmonic metal nanoparticles to form hybrid compounds. The resulting structures display unique features arising from the combination of the individual properties of both materials, such as the plasmonic optical effects of metal nanoparticles and the physicochemical properties of 2D materials. Metals such as Au, Ag, or Cu are provided light absorption in the UV-visible and NIR range and a high charge-carrier concentration so that they can support an intrinsic strong plasmonic effect [68]: when plasmonic materials are incorporated into a hybrid compound, the plasmonic effect is introduced in the structure, providing the capability to overcome the issue of the reduced light absorption. As a result of the plasmonic effect induced by the metal nanomaterial in the hybrid structure, some properties will be modified and improved. As a result of the combination of the two materials, the electric field at the interface is enhanced, and the charge transfer between plasmonic metal and probe molecules is increased as a consequence of the high carrier mobility. In this context, the plasmonic effect results in plasmon-induced "hot electrons", improving the conductivity of the hybrid nanostructures and enhancing the photogeneration rate [2]. Bidimensional nanomaterials offer additional advantages, such as a large surface area and enhanced functional groups providing numerous active sites for the interactions with other molecules as well as the capability to bind protein and nucleic acid via π–π stacking interactions with aromatic rings, resulting in a larger number of molecules adsorbed on the nanocomposite surface, improving their performances in biosensing applications [69]. In the present work, an overview on colorimetric assays based on the outstanding properties of hybrid nanoparticles/2D nanomaterials will be given.

### *5.2. Catalysis of Hybrid Compounds toward 4-NP Reduction*

Investigation of the catalytic performance of semiconducting TMDs hybridized with plasmonic metal nanoparticles toward the reduction of 4-nitrophenol (4-NP) to 4-aminophenol (4-AP) has been performed considering disulfide of tungsten, $WS_2$, which is one of the most representative compounds of this class of materials. A first approach in the use of AgNPs@$WS_2$ nanosheets as catalyst has been reported in the work of Lee [70]. Here, after the exfoliation of bulk $WS_2$, AgNPs were readily introduced onto the $WS_2$ nanosheets via an amine-assisted in situ growth method with a control on the particle size. The AgNPs with different sizes supported on $WS_2$ nanosheets were used to photocatalyze the reduction of 4-nitrophenol (4-NP) to 4-aminophenol (4-AP) under visible light irradiation in order to evaluate the catalytic efficiency. The Ag@$WS_2$ hybrid material was added to a 4-NP aqueous solution, whereafter it was irradiated with an LED lamp. Monitoring the reaction by means of UV-visible spectroscopy allows us to observe that as the reaction progressed, the peak at 400 nm of 4-NP disappears, while a new peak corresponding to the product (4-AP) appears at 300 nm. Three different sizes of the AgNPs have been tested: smaller particles (sAgNPs), large nanoparticles (LAgNPs) and bigger AgNPs (XLAgNPs), and the obtained results showed that large nanoparticles (LAgNPs) exhibit higher activity in the reduction reaction under visible light irradiation ($k = 0.178\ min^{-1}$) compared to smaller particles (sAgNPs with $k = 0.014\ min^{-1}$) and bigger particles (XLAgNPs). X-ray photoelectron spectroscopy (XPS) analysis shows that in sAgNPs@$WS_2$ hybrids, most of the Ag atoms were monovalent ($Ag^+$), whereas in LAgNPs@$WS_2$ nanohybrids, most of the Ag atoms were zerovalent ($Ag^0$). Thus, the enhanced catalytic efficiency for LAgNPs@$WS_2$ is explained by the different oxidation state of Ag, with $Ag^0$ atoms having the highest activity, thus suggesting that the surface state

of the catalyst determines the photocatalytic activity. In case of XLAgNPs@$WS_2$ hybrids, the lower activity has been explained by the shielding of the photoactive sites on $WS_2$ nanosheets. Comparing the results obtained with the catalytic efficiency of other photocatalytic systems, it has been found that nanohybrids showed two or three orders of magnitude higher values of turnover frequency (TOF). The enhancement of the catalytic activity has been attributed to the increased density of electrons of AgNPs on the nanohybrids via excited electron transfer from the semiconducting $WS_2$. In a successive work [71], hybrid nanosystems composed of a cationic polymer, (poly(diallyldimethylammonium chloride) (PDDA)-stabilized $WS_2$ nanosheets and Au nanoparticles (AuNPs) have been tested as catalysts for 4-NP reduction. Bulk $WS_2$ has been exfoliated by means of PDDA, and the obtained few-layer $WS_2$ nanosheets (less than three layers), PDDA-FL-$WS_2$-NSs, successively have been decorated with negative citrate-capped Au, Pd, and Pt nanoparticles via electrostatic interactions, and their catalytic efficiency evaluated. As in the previous work, the reduction of 4-NP has been monitored by UV-visible spectroscopy, and comparing the three different types of metal nanoparticles, it has been found that nanocomposites of PdNPs and PDDA-FL-$WS_2$-NSs showed the higher catalytic efficiency. In addition, all the hybrid systems showed an enhancement in catalytic activity compared to the bare metal nanoparticles, which was due to the presence of the $WS_2$ nanosheets. In Figure 4, a schematic of 4-NP reduction is shown.

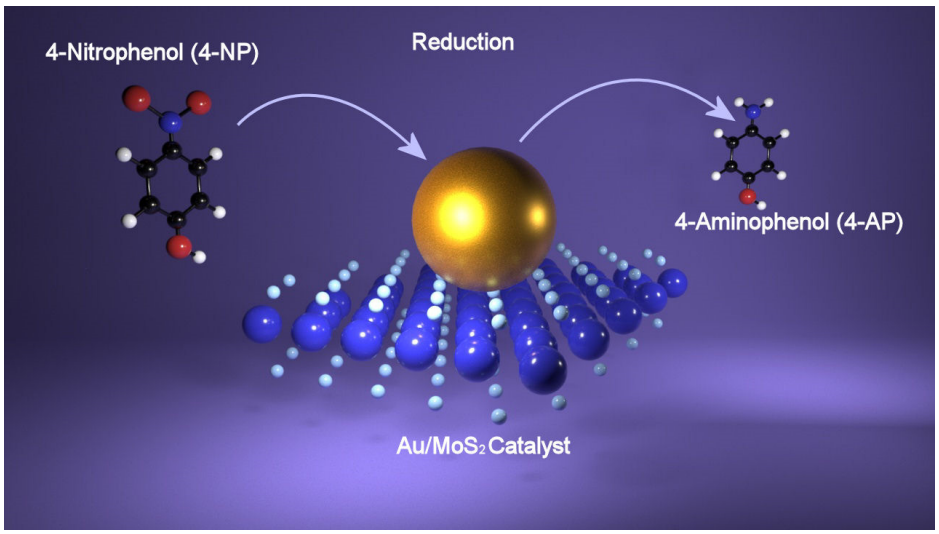


**Figure 4.** Reduction of 4-nitrophenol (4-NP) catalyzed by Au-$MoS_2$ nanohybrid by which 4-aminophenol (4-AP) is obtained.

## 6. Hybrid Compounds for Colorimetric Detection

In this section, the applications of hybrid metal nanoparticles/2D nanomaterials in the colorimetric detection of molecules, motivated by their outstanding properties such as peroxidase-like activity and LSPR, will be reviewed.

### *6.1. Colorimetric Detection Based on LSPR of Hybrid Compounds*

Stimulated by marvelous optoelectronic plasmonic properties, in his work, Wu [72] decorated $MoS_2$ nanosheets with gold nanoparticles (AuNPs), obtaining a hybrid system exhibiting outstanding optical properties, which has been investigated for the detection of 2,4,6-trinitrotoluene (TNT), which is an explosive. Because $MoS_2$ showed a great redox behavior, thus being able to reduce metal precursor, the hybrid systems composed of $MoS_2$ nanosheets decorated with Au nanoparticles (AuNps@$MoS_2$) were obtained, adding the solution of gold salt to a solution of $MoS_2$ nanosheets and heating the mixture thus obtained. Successively, the AuNPs@$MoS_2$ hybrid systems have been functionalized with the bio-recognition elements: explosive-specific peptides. Following the covalent binding between Au nanoparticles and the sulfhydryl group of TNT-specific peptides, a red-shift of the absorption peak is observed. The peptide chains functionalizing the AuNPs@$MoS_2$ hybrid

are able to bind TNT molecules via the donor–acceptor interactions between tryptophan and TNT, π–π interactions between histidine and TNT and partial charge–charge interactions or hydrogen bonds between imidazole side chains in peptides and nitro groups in TNT molecules, thus, upon adding a TNT, changes in absorption spectra have been observed as a consequence of peptide binding with TNT molecules. A further red-shift of 4 nm following the TNT binding with peptides is observed, but in particular, the intensity of the absorption peak decreases when TNT concentration increases, so fitting the absorbance intensity of the peak at 541 nm with TNT concentration, a linear relation is obtained, which can be used for quantitative analysis. From the results, it has been found that the sensing platform could detect TNT at the concentration as low as $2 \times 10^{-7}$ M. In order to further investigate the sensing performances of the Au Nps@$MoS_2$ hybrid, TNT molecules have been detected using peptide-functionalized Au nanoparticles and pristine $MoS_2$, and the results obtained confirmed the enhanced sensitivity of Au Nps@$MoS_2$ systems, magnifying the response to TNT molecules. In Figure 5, the TNT sensing by means of LSPR is shown.

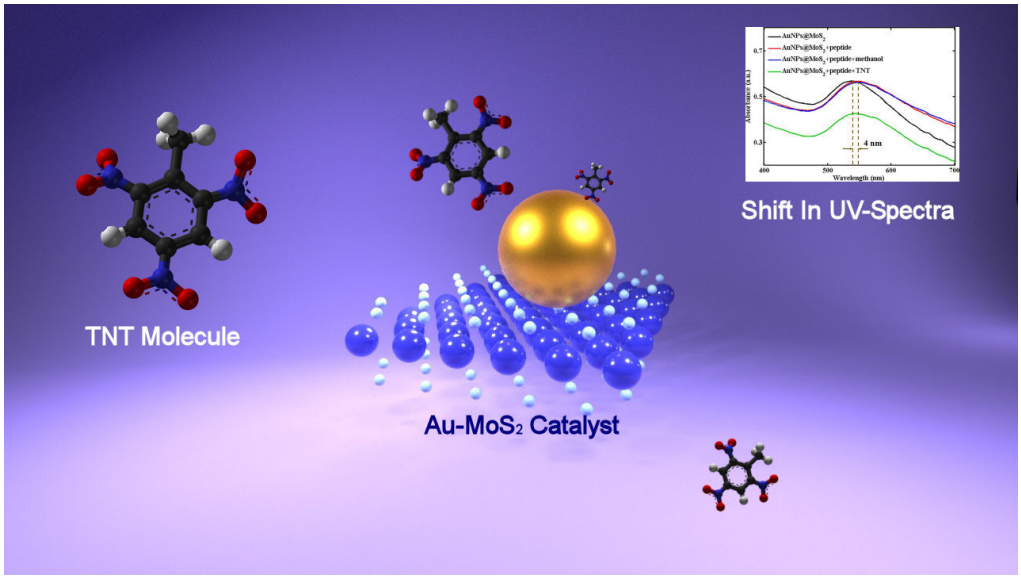


**Figure 5.** TNT sensing by monitoring the shifts of LSPR peak in the UV spectra.

*6.2. Colorimetric Sensing Based on Peroxidase-Like Activity*

The previous work of Guo [39,40] showed the potential of exploiting the peroxidase-like activity of bidimensional nanomaterial in the colorimetric detection, but in the work of Saxena [73], there was a detailed explanation for a plausible mechanism behind TMB reduction with $H_2O_2$ reaction in the presence of $MoS_2$ and Au-$MoS_2$ nanocomposites as catalysts. The lone pair of electrons in the amino group of TMB is localized in the non-bonding orbital of the molecule (NBO), and in the absence of a catalyst, the energy of the LUMO of $H_2O_2$ is higher compared to that of NBO, so the electrons cannot be transferred from the NBO of TMB. When adding a catalyst to a mixture of TMB and $H_2O_2$, in the UV spectra, the characteristic absorption peaks of the 1 electron charge transfer complex of TMB start to appear and the system turns into a blue color, thus validating the electron transfer from the NBO of TMB to the catalyst. When using $MoS_2$ as catalyst and electrons are acquired from TMB, the Fermi level of $MoS_2$ rises in energy, thus enabling the sequential electron transfer to LUMO of $H_2O_2$ by which $H_2O_2$ is reduced and ·OH radicals are generated. At a higher increase in the catalyst's Fermi energy when receiving electrons from TMB, the driving force of $H_2O_2$ reduction is larger, resulting in a faster reaction. In addition, the transfer of electrons from TMB to the Fermi level confirms the catalytic activity of $MoS_2$ that can be assigned to its p-type nature [74]. Furthermore, exploiting the hybrid compound formed by Au nanoparticles and $MoS_2$ nanomaterials, a superior peroxidase-like activity has been demonstrated. Due to the thermal excitation of Au NPs

occurring spontaneously at the heterointerface between $MoS_2$ and Au, the thermal electrons localized in the AuNPs can transfer to the surrounding $MoS_2$ nanosheets, so that when the hybrid compound receives electrons from TMB, the increase in its Fermi energy is higher compared to that of $MoS_2$ nanosheets, thus improving the catalytic activity [42]. At this point, the so-produced ·OH radicals react with TMB molecules, the electrons are transferred to the catalyst and the oxidized form of TMB is produced. In Figure 6, the reduction in TMB in the presence of Au-$MoS_2$ is represented.

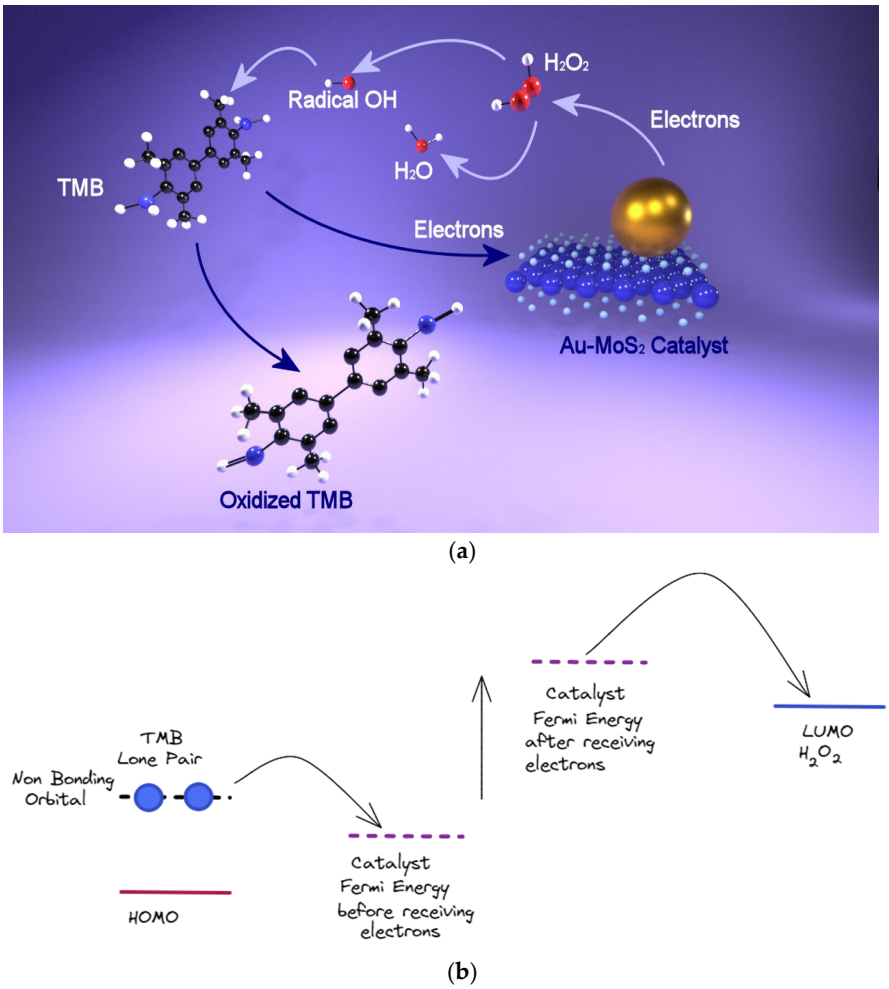


**Figure 6.** (**a**) Plausible mechanism for the peroxidase-like activity of the hybrid compounds; (**b**) energetics levels for the catalysis.

Stimulated by the extraordinary catalytic properties of the nanocomposites, a colorimetric assay based on the peroxidase-like activity of molybdenum disulfide ($MoS_2$) nanosheets hybridized with gold nanoparticles ($MoS_2$-Au) has been developed by Zhang [75] to detect $Hg^+$ ions in a system. After producing $MoS_2$-Au nanocomposites with a microwave-assisted solvothermal method, a first test to evaluate the catalytic activity toward the oxidation of 3,3′,5,5′-tetramethylbenzidine (TMB) with $H_2O_2$ has been performed, finding a linear response in the range 20 nM to 20 µM and a detection limit (LOD) of 5 nM. In a successive test, traces of $Hg^+$ ions have been added into the reaction system, resulting in a rapid stimulation of the $MoS_2$-Au nanocomposites' peroxidase-like activity. The Michaelis–Menten constant (Km) represents the affinity of a given enzyme toward the substrate: the smaller Km value means the stronger affinity between the enzyme and the substrate, thus, in order to evaluate the $Hg^{2+}$-stimulation effect on the peroxidase-like activity of $MoS_2$-Au, Km has been calculated without and with $Hg^+$ ions. As a result, the values of Km are lower in the presence of $Hg^+$ ions, thus confirming the stimulation effect of mercury. The stimulation effect has been assigned

to the formation of a Au-Hg amalgam, promoting the strong interaction between $Hg^{2+}$ and $MoS_2$-Au. In addition, it has been found that the catalytic activity stimulation is dependent on $Hg^+$ concentration, so that when the $Hg^+$ concentration rises, the absorbance peak in the UV-Vis spectra of oxTMB at 652 nm increases. As a result, from the calibration curve obtained plotting $\Delta A$ ($\Delta A = A - A_0$, with A and $A_0$ representing the absorbance at 652 nm in the presence and absence of $Hg^{2+}$) vs. [$Hg^+$], we obtain a linear relationship and an LOD of 5 nM, which is much lower compared to previous work. The reaction can be visually followed with the naked eye: in the absence of a catalyst, the reagent solution is colorless, and when adding the $MoS_2$-Au nanocomposites, a deep blue color starts to appear. Accordingly, in the UV-visible spectra the absorbance at 652 nm increased when the $Hg^+$ concentration in the system was raised. Finally, the so-developed colorimetric assay has been successfully applied to detect $Hg^+$ ions in tap water, showing an excellent activity toward interfering ions. Because of the extraordinary performances, the developed colorimetric assay holds great potential in environmental protection and monitoring. The peroxidase-like activity of hybrid nanocomposites has been exploited to detect cadmium, cholesterol and also $H_2O_2$ as well as cancer cells [42,73,76].

### *6.3. Colorimetric Sensing Based on Catalysis of Reduction Reaction of 4NP*

In the work of Wang [77], a colorimetric sensor for carcinoembryonic antigen (CEA), a tumor biomarker, has been developed on the basis of the excellent catalytic activity of $MoS_2$ nanosheets hybridized with AuNPs. The so-developed platform sensing is a "sandwich" immunocomplex where the first layer of the structure is formed by molybdenum disulfide ($MoS_2$) nanosheets hybridized with AuNPs conjugated with anti-CEA (Ab1-$MoS_2$-AuNPs). This layer is used to capture the CEA target; therefore, it has been made to react with bovine serum albumin (BSA) to block the sites still active in order to hinder nonspecific adsorption. The Ab1-$MoS_2$-AuNPs composite has been made to react with CEA, and successively, from the reaction of the so-obtained CEA-Ab1-$MoS_2$-AuNPs with Ab2-$MoS_2$-AuNPs, the "sandwich immunocomplex" is obtained. The Ab2-$MoS_2$-AuNPs layer maintains its catalytic activity because it has not reacted with BSA. After this last reaction, the solution has been centrifugated, and the supernatant was collected. When the supernatant is added to a solution of 4-nitrophenol (4-NP) and sodium borohydride ($NaBH_4$), the Ab2-$MoS_2$-AuNPs composites advanced from the immunocomplex formation and catalyzed the reaction 4-NP + $NaBH_4$ $\rightarrow$ 4-AP (4-aminophenol). The 4-NP solution is pale yellow, showing a peak centered at about 317 nm in the UV-Vis spectra; adding $NaBH_4$, the solution turns to bright yellow, and in the UV-Vis spectrum, a peak is present at about 400 nm, which is the nitrophenolate ion peak. Finally, when adding the supernatant containing the Ab2-$MoS_2$-AuNPs composites, the 4-NP and $NaBH_4$ solution turns colorless from bright yellow, indicating that the reaction 4-NP + $NaBH_4$ $\rightarrow$ 4-AP has occurred. When adding the Ab2-$MoS_2$-AuNPs nanohybrid, in the UV-Vis spectra, the intensity of the peak at 400 nm decreases, while the intensity at 300 nm (4-AP) increases. Increasing the amount of CEA in the immunocomplex formation, the Ab2-$MoS_2$-AuNPs nanohybrid quantity in the supernatant decreases along as with the catalytic activity so that a linear relation between absorbance at 400 nm and logarithm of CEA concentration (Log [CEA]) for [CEA] comprised in the range 5 pg/mL–10 ng/mL has been found from which a Limit of Detection (LOD) of 0.5 pg/mL has been calculated. The value of LOD has been compared with that obtained in other works for other colorimetric platforms, finding improved performances [78–80]. In addition, the catalytic activity has been evaluated by the time of the catalytic reduction reaction, finding that the reaction is complete in 680 s, 420 s, 240 s, and 200 s exploiting $MoS_2$ nanosheets, AuNPs, Ab2-$MoS_2$-AuNPs and $MoS_2$-AuNPs nanocomposites as catalysts, thus demonstrating the outstanding catalytic activity of the hybrid systems. The Ab2-$MoS_2$-AuNPs has demonstrated a slightly lower catalytic activity compared to the $MoS_2$-AuNPs because the antibodies adsorbed on the surface hindered the catalytic activity of Ab2-$MoS_2$-AuNPs nanocomposites. The excellent catalytic activity of the hybrid systems has been motivated by means of three factors. Firstly, thanks to the

large surface area, the nanohybrids are able to absorb a higher number of 4-NP molecules by means of π–π stacking, thus increasing the reactant concentration near the catalyst and so facilitating the catalysis process. Secondly, the AuNPs agglomeration is prevented by using the $MoS_2$ nanosheets as a substrate, so that their catalytic efficiency is maintained. Thirdly, the catalytic reaction is promoted by both AuNPs and $MoS_2$ nanosheets.

Table 1 contains a summary of the different colorimetric sensing based on hybrid compounds.

**Table 1.** Different colorimetric detection strategies based on 2D nanomaterials and hybrid compounds with plasmonic metal nanoparticles.

| Catalyst | Detection Strategy | Detected Molecule | Limit of Detection (LOD) | Reference |
|---|---|---|---|---|
| **$MoS_2$** | Peroxidase-like activity | Glucose | 1.2 μmol $L^{-1}$ | [39] |
| **$WS_2$** | Peroxidase-like activity | Glucose | 2.9 μM | [40] |
| **$MoS_2$–Au nanocomposites** | Peroxidase-like activity | $Hg^{2+}$ ions | 5 nM | [75] |
| **Au–$MoS_2$ nanocomposites** | Peroxidase-like activity | Cadmium | 0.7 ng/mL | [76] |
| **Molybdenum disulfide nanoribbons hybridized with AuNPs ($MoS_2$ NRs–AuNPs)** | Peroxidase-like activity | Cholesterol | 0.015 mM | [73] |
| **$MoS_2$/C-$Au_{600}$** | Peroxidase-like activity | Cancer cells | | [42] |
| **Nanocomposites of gold nanoparticles and 2D $MoS_2$sheets (AuNPs@$MoS_2$)** | LSPR shifts | 2,4,6-trinitrotoluene (TNT) | $4 \times 10^{-6}$ M | [72] |
| **$MoS_2$-AuNPs nanocomposites** | Reduction in 4-NP | Carcinoembryonic antigen (CEA) | 0.5 pg/mL | [77] |

## 7. Future Perspectives

Several point-of-care (POC) devices have been developed in the last few years, including microfluidic, paper-based, consumer electronic plasmonic devices, and so on [81]. One of the most famous is the test for SARS-CoV-2 detection, which is based on the colorimetric detection of Au nanoparticles, but despite the progress, the research on the application of the hybrid systems in colorimetric assays to be implemented in POC is only in the early stage. In addition, sensing techniques and optical imaging based on smartphones have gained increasing interest, which is motivated by the high sensitivity and image resolution achieved while removing the need for costly and bulky optical instrumentation. Taking advantage of the built-in camera, screen/flash, and the connection to data storage capabilities available in the "cloud", smartphones or tablets provide an appealing and low-cost alternative to bulky optical instrumentation, so that incorporating a sensing system into a smartphone by means of different accessories reveals a promising approach to permit the application of smartphones to sense, transduce, and communicate different types of biological information. As an example, by adding small field-portable fluorescence microscopy accessories to a smartphone, it has been possible to image individual fluorescent nanoparticles and viruses with diameters down to 100 nm [82]. In addition, by incorporating commercially available lens systems, it is possible to image cells, bacteria and biological tissue at 350× magnification [83]. In the work of Liedberg [84], a portable smartphone spectrometer to monitor optical changes in real time has been developed and applied as an LSPR biosensor by designing an assay for cardiac human troponin (troponin I), the heart disease biomarker, exploiting AuNPs. By measuring the absorbance peak of the AuNPs and exploiting the smartphone as a spectrometer, it has been possible to detect troponin. A simulation study showing that LSPR color filters can be exploited for a low-cost reading set-up has been performed very recently by Fantoni et al. [85]. In a first step, the light transmission properties of a transparent substrate covered with a layer of uniformly distributed Au nanoparticles with and without the combination of different 2D nanomaterials have been simulated, and then, the results obtained were transformed

into a vector in XYZ, Lab, and RGB color spaces. The principal finding is a quantification of how much, and in which manner, the color recognition process may be affected by different parameters, and once optimized, the digital camera of a mobile phone would be suitable for the implementation of this method, paving the way to low-cost sensing. In this context, it has been proposed that the photo camera of a smartphone would be the best target to implement this method, thus paving the way for the use of the plasmonic metal nanoparticles/2D nanomaterials hybrids as a sensing platform combined with an innovative output reading requiring just a smartphone in point of care devices such as for example the acute kidney disease or the viral surface spike proteins of SARS-CoV-2. Figure 7 shows a schematic of the detection mechanism.

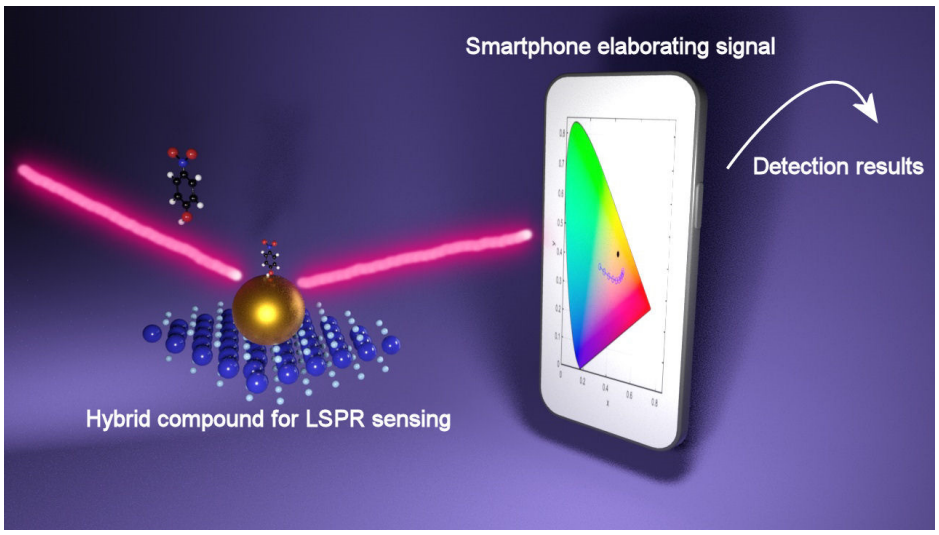


**Figure 7.** Recognition process of LSPR signal provided by smartphone (from Ref. [52]).

## 8. Conclusions

In this work, firstly, the characteristics of plasmonic metal nanoparticles and 2D nanomaterials have been discussed separately in order to gain a better understanding of the properties of the hybrid compounds generated from the combinations of the two structures. After a critical review of the strategies at the basis of colorimetric sensing, the exceptional properties displayed from the hybrids and originating from the synergistic effect of the individual part of the structure have been discussed along with their use to develop colorimetric assays. The achieved progress has prepared the ground for the integration of the hybrid plasmonic metal nanoparticles/2D nanomaterials in the next-generation diagnostic tools so that the issues related to the development of PoC devices have been critically discussed, considering the limitations and challenges that must be overcome for their full implementation with the aim of helping the development of more advanced sensing devices.

**Author Contributions:** Conceptualization, C.S., A.F. and E.C.B.A.A.; writing—original draft preparation, C.S.; writing—review and editing, C.S., A.F. and E.C.B.A.A.; supervision, M.V., A.F. and E.C.B.A.A.; project administration, A.F. and E.C.B.A.A.; funding acquisition, M.V., A.F. and E.C.B.A.A. All authors have read and agreed to the published version of the manuscript.

**Funding:** This research was supported by EU funds through the FEDER European Regional Development Fund project LISBOA-01-0145-FEDER-031311, by Portuguese national funds provided by FCT—Fundação para a Ciência e Tecnologia, through grant SFRH/BD/09347/2021, PTDC/NANOPT/31311/2017, PTDC/QUI-QIN/29778/2017 and UID/EEA/00066/2020 projects and Instituto Politécnico de Lisboa (IPL/2021/WASTE4CAT_ISEL and IPL/2021/MuMiAS-2D_ISEL).

**Conflicts of Interest:** The authors declare no conflict of interest.

## References


1. Zhou, P.; Yang, X.L.; Wang, X.G.; Hu, B.; Zhang, L.; Zhang, W.; Si, H.R.; Zhu, Y.; Li, B.; Huang, C.L.; et al. A pneumonia outbreak associated with a new coronavirus of probable bat origin. *Nature* **2020**, *579*, 270–273. [CrossRef] [PubMed]
2. Soler, M.; Huertas, C.S.; Lechuga, L.M. Label-free plasmonic biosensors for point-of-care diagnostics: A review. *Expert Rev. Mol. Diagn.* **2019**, *19*, 71–81. [CrossRef] [PubMed]
3. Mejía-Salazar, J.R.; Osvaldo, N.O. Plasmonic Biosensing (Focus Review). *Chem. Rev.* **2018**, *118*, 10617–10625. [CrossRef] [PubMed]
4. Han, X.; Liu, K.; Sun, C. Plasmonics for Biosensing. *Materials* **2019**, *12*, 1411. [CrossRef]
5. Liu, J.; Jalali, M.; Mahshid, S.; Wachsmann-Hogiu, S. Are plasmonic optical biosensors ready for use in point-of-need applications? *Analyst* **2020**, *145*, 364–384. [CrossRef]
6. De, M.; Ghosh, P.S.; Rotello, V.M. Applications of Nanoparticles in Biology. *Adv. Mater.* **2008**, *20*, 4225–4241. [CrossRef]
7. Stewart, M.E.; Anderton, C.R.; Thompson, L.B.; Maria, J.; Gray, S.K.; Rogers, J.A.; Nuzzo, R.G. Nanostructured Plasmonic Sensors. *Chem. Rev.* **2008**, *108*, 494–521. [CrossRef]
8. Feng, X.; Liu, L.; Wang, S.; Zhu, D. Water-soluble fluorescent conjugated polymers and their interactions with biomacromolecules for sensitive biosensors. *Chem. Soc. Rev.* **2010**, *39*, 2411–2419. [CrossRef]
9. Rosi, N.L.; Mirkin, C.A. Nanostructures in Biodiagnostics. *Chem. Rev.* **2005**, *105*, 1547–1562. [CrossRef]
10. Zhao, W.; Brook, M.A.; Li, Y. Design of Gold Nanoparticle-Based Colorimetric Biosensing Assays. *ChemBioChem* **2008**, *9*, 2363–2371. [CrossRef]
11. Gao, L.; Zhuang, J.; Nie, L.; Zhang, J.; Zhang, Y.; Gu, N.; Wang, T.; Feng, J.; Yang, D.; Perrett, S.; et al. Intrinsic peroxidase-like activity of ferromagnetic nanoparticles. *Nat. Nanotech.* **2007**, *2*, 577–583. [CrossRef] [PubMed]
12. Asati, A.; Santra, S.; Kaittanis, C.; Nath, S.; Perez, J.M. Oxidase-Like Activity of Polymer-Coated Cerium Oxide Nanoparticles. *Angew. Chem. Int. Ed.* **2009**, *48*, 2308–2312. [CrossRef] [PubMed]
13. Song, Y.J.; Qu, K.G.; Zhao, C.; Ren, J.S.; Qu, X.G. Graphene Oxide: Intrinsic Peroxidase Catalytic Activity and Its Application to Glucose Detection. *Adv. Mater.* **2010**, *22*, 2206–2210. [CrossRef] [PubMed]
14. Sriram, P.; Manikandan, A.; Chuang, F.; Chueh, Y. Hybridizing Plasmonic Materials with 2D-Transition Metal Dichalcogenides toward Functional Applications. *Small* **2020**, *16*, 1904271. [CrossRef]
15. Li, X.; Zhu, J.; Wei, B. Hybrid nanostructures of metal/two-dimensional nanomaterials for plasmon-enhanced applications. *Chem. Soc. Rev.* **2016**, *45*, 3145–3187. [CrossRef]
16. Zhu, D.; Liu, B.; Wei, G. Two-Dimensional Material-Based Colorimetric Biosensors: A Review. *Biosensors* **2021**, *11*, 259. [CrossRef]
17. Estevez, M.C.; Otte, M.A.; Sepulveda, B.; Lechuga, L.M. Trends and challenges of refractometric nanoplasmonic biosensors: A review. *Anal. Chim. Acta* **2014**, *806*, 55–73. [CrossRef]
18. Chen, Y.; Ming, H. Review of surface plasmon resonance and localized surface plasmon resonance sensor. *Photonic Sens.* **2012**, *2*, 37–49. [CrossRef]
19. Sambles, J.R.; Bradbery, G.W.; Yang, F.Z. Optical-excitation of surface-plasmons—An introduction. *Contemp. Phys.* **1991**, *32*, 173–183. [CrossRef]
20. Moznuzzaman, M.; Islam, M.R.; Hossain, M.B. Mehedi IM Modeling of highly improved spr sensor for formalin detection. *Resul. Phys.* **2020**, *16*, 102874. [CrossRef]
21. Soler, M.; Lechuga, L.M. Principles, technologies, and applications of plasmonic biosensors. *J. Appl. Phys.* **2021**, *129*, 111102. [CrossRef]
22. Barnes, W.L.; Dereux, A.; Ebbesen, T.W. Surface plasmon subwavelength optics. *Nature* **2003**, *424*, 824–830. [CrossRef] [PubMed]
23. Mosier-Boss, P.A. Review of SERS Substrates for Chemical Sensing. *Nanomaterials* **2017**, *7*, 142. [CrossRef] [PubMed]
24. Nie, W.; Wang, Q.; Yang, X.; Zhang, H.; Li, Z.; Gao, L.; Zheng, Y.; Liu, X.; Wang, K. High sensitivity surface plasmon resonance biosensor for detection of microRNA based on gold nanoparticles-decorated molybdenum sulfide. *Anal. Chim. Acta* **2017**, *993*, 55–62. [CrossRef]
25. Wriedt, T. Mie theory: A review. In *the Mie Theory*; Hergert, W., Wriedt, T., Eds.; Springer: Berlin, Germany, 2012; pp. 53–71.
26. Mie, G. Beiträge zur Optik trüber Medien, speziell kol-loidaler Metallösungen. *Ann. Phys.* **1908**, *25*, 377–445. [CrossRef]
27. Maier, S.A. *Plasmonics: Fundamentals and Applications*; Springer: New York, NY, USA, 2007.
28. Farooq, S.; de Araujo, R.E. Engineering a Localized Surface Plasmon Resonance Platform for Molecular Biosensing. *Open J. Appl. Sci.* **2018**, *8*, 126–139. [CrossRef]
29. Fleischmann, M.; Hendra, P.J.; Mc Quillan, A.J. Raman spectra of pyridine adsorbed at a silver electrode. *Chem. Phys. Lett.* **1974**, *26*, 163–166. [CrossRef]
30. Albrecht, M.G.; Creighton, J.A. Anomalously intense Raman spectra of pyridine at a silver electrode. *J. Am. Chem. Soc.* **1977**, *99*, 5215–5217. [CrossRef]
31. Jeanmaire, D.L.; van Duyne, R.P. Surface raman spectroelectrochemistry: Part I. Heterocyclic, aromatic, and aliphatic amines adsorbed on the anodized silver electrode. *J. Electroanal. Chem. Interfacial Electrochem.* **1977**, *84*, 1–20. [CrossRef]
32. Serafinelli, C.; Fantoni, A.; Alegria, E.C.B.A.; Vieira, M. Plasmonic Metal Nanoparticles Hybridized with 2D Nanomaterials for SERS Detection: A Review. *Biosensors* **2022**, *12*, 225. [CrossRef]
33. Das, A.; Choi, N.; Moon, J.; Choo, J. Determination of total iron-binding capacity of transferrin using metal organic framework-based surface-enhanced Raman scattering spectroscopy. *J. Raman Spectrosc.* **2021**, *52*, 506–515. [CrossRef]

34. Kolobov, A.V.; Bulk, T.J. TMDCS: Review of Structure and Properties. In *Two-Dimensional Transition-Metal Dichalcogenides*; Springer: Cham, Switzerland, 2016; pp. 29–77.
35. Hu, Y.; Huang, Y.; Tan, C.; Zhang, X.; Lu, Q.; Sindoro, M.; Huang, X.; Huang, W.; Wang, L.; Zhang, H. Two-dimensional transition metal dichalcogenide nanomaterials for biosensing applications. *Mater. Chem. Front.* **2017**, *1*, 24–36. [CrossRef]
36. Manzeli, S.; Ovchinnikov, D.; Pasquier, D.; Yazyev, O.V.; Kis, A. 2D transition metal dichalcogenides. *Nat. Rev. Mater.* **2017**, *2*, 17033. [CrossRef]
37. Kuc, A.; Zibouche, N.; Heine, T. Influence of quantum confinement on the electronic structure of the transition metal sulfide TS2. *Phys. Rev. B* **2011**, *83*, 245213. [CrossRef]
38. Splendiani, A.; Sun, L.; Zhang, Y.; Li, T.; Kim, J.; Chim, C.Y.; Galli, G.; Wang, F. Emerging photoluminescence in monolayer MoS2. *Nano Lett.* **2010**, *10*, 1271–1275. [CrossRef]
39. Lin, T.; Zhong, L.; Guo, L.; Fu, F.; Chen, G. Seeing diabetes: Visual detection of glucose based on the intrinsic peroxidase-like activity of MoS2 nanosheets. *Nanoscale* **2014**, *6*, 11856–11862. [CrossRef]
40. Lin, T.; Zhong, L.; Song, Z.; Guo, L.; Wu, H.; Guo, Q.; Chen, Y.; Fu, F.; Chen, G. Visual detection of blood glucose based on peroxidase-like activity of WS2 nanosheets. *Biosens. Bioelectron.* **2014**, *62*, 302–307. [CrossRef]
41. Guardia, L.; Paredes, J.I.; Munuera, J.M.; Villar-Rodil, S.; Ayán-Varela, M.; Martínez-Alonso, A.; Tascón, J.M. Chemically Exfoliated MoS2 Nanosheets as an Efficient Catalyst for Reduction Reactions in the Aqueous Phase. *ACS Appl. Mater. Interfaces* **2014**, *6*, 21702–21710. [CrossRef]
42. Sun, H.; Gao, Y.; Hu, N.; Zhang, Y.; Guo, C.; Gao, G.; Ma, Z.; Ivanovich, K.I.; Qiu, Y. Electronic coupling between molybdenum disulfide and gold nanoparticles to enhance the peroxidase activity for the colorimetric immunoassays of hydrogen peroxide and cancer cells. *J. Colloid Interface Sci.* **2020**, *578*, 366–378. [CrossRef]
43. Nirala, N.R.; Prakash, R. One step synthesis of AuNPs@MoS2-QDs composite as a robust peroxidase- mimetic for instant unaided eye detection of glucose in serum, saliva and tear. *Sens Actuators B Chem.* **2018**, *263*, 109–119.
44. Polavarapu, L.; Pérez-Juste, J.; Xu, Q.; Liz-Marzán, L.M. Optical sensing of biological, chemical and ionic species through aggregation of plasmonic nanoparticles. *J. Mater. Chem. C* **2014**, *2*, 7460–7476. [CrossRef]
45. Mirkin, C.A.; Letsinger, R.L.; Mucic, R.C.; Storhoff, J.J. A DNA-based method for rationally assembling nanoparticles into macroscopic materials. *Nature* **1996**, *382*, 607–609. [CrossRef] [PubMed]
46. Min Zhang Yu-Qiang Liu Bang-Ce, Y.e. Colorimetric assay for parallel detection of Cd2+, Ni2+ and Co2+ using peptide-modified gold nanoparticles. *Analyst* **2012**, *137*, 601–607.
47. Wen, S.; Zheng, F.; Shen, M.; Shi, X. Synthesis of polyethyleneimine-stabilized gold nanoparticles for colorimetric sensing of heparin. *Colloids Surf. A Physicochem. Eng. Asp.* **2013**, *419*, 80–86. [CrossRef]
48. Pramanik, A.; Gao, Y.; Patibandla, S.; Gates, K.; Ray, P.C. Bioconjugated Nanomaterial for Targeted Diagnosis of SARS-CoV-2. *Acc. Mater. Res.* **2022**, *3*, 134–148. [CrossRef]
49. Moitra, P.; Alafeef, M.; Dighe, K.; Frieman, M.B.; Pan, D. Selective Naked-Eye Detection of SARS-CoV-2 Mediated by N Gene Targeted Antisense Oligonucleotide Capped Plasmonic Nanoparticles. *ACS Nano* **2020**, *14*, 7617–7627. [CrossRef]
50. Santillán, J.M.J.; Videla, F.A.; Scaffardi, L.B.; Schinca, D.C. Plasmon Spectroscopy for Subnanometric Copper Particles: Dielectric Function and Core–Shell Sizing. *Plasmonics* **2013**, *8*, 341–348. [CrossRef]
51. Laghari, G.N.; Nafady, A.; Al-Saeedi, S.I.; Sherazi, S.T.; Nisar, J.; Shah, M.R.; Abro, M.I.; Arain, M.; Bhargava, S.K. Bhargava. Ranolazine-Functionalized Copper Nanoparticles as a Colorimetric Sensor for Trace Level Detection of As3+. *Nanomaterials* **2019**, *9*, 83. [CrossRef]
52. Guo, Y.; Wu, J.; Li, J.; Ju, H. A plasmonic colorimetric strategy for biosensing through enzyme guided growth of silver nanoparticles on gold nanostars. *Biosens. Bioelectron.* **2016**, *78*, 267–273. [CrossRef]
53. Xu, S.; Jiang, L.; Liu, Y.; Liu, P.; Wang, W.; Luo, X. A morphology-based ultrasensitive multicolor colorimetric assay for detection of blood glucose by enzymatic etching of plasmonic gold nanobipyramids. *Anal. Chim. Acta* **2019**, *1071*, 53–58. [CrossRef]
54. Soares, L.; Csáki, A.; Jatschka, J.; Fritzsche, W.; Flores, O.; Franco, R.; Pereira, E. Localized surface plasmon resonance (LSPR) biosensing using gold nanotriangles: Detection of DNA hybridization events at room temperature. *Analyst* **2014**, *139*, 4964–4973. [CrossRef] [PubMed]
55. Shiohara, A.; Langer, J.; Polavarapu, L.; Liz-Marzán, L.M. Solution processed polydimethylsiloxane/gold nanostar flexible substrates for plasmonic sensing. *Nanoscale* **2014**, *6*, 9817–9823. [CrossRef] [PubMed]
56. Tadepalli, S.; Kuang, Z.; Jiang, Q.; Liu, K.K.; Fisher, M.A.; Morrissey, J.J.; Kharasch, E.D.; Slocik, J.M.; Naik, R.R.; Singamaneni, S. Peptide Functionalized Gold Nanorods for the Sensitive Detection of a Cardiac Biomarker Using Plasmonic Paper Devices. *Sci. Rep.* **2015**, *5*, 1–11.
57. Mohamad, A.; Teo, H.; Keasberry, N.A.; Ahmed, M.U. Recent developments in colorimetric immunoassays using nanozymes and plasmonic nanoparticles. *Crit. Rev. Biotechnol.* **2019**, *39*, 50–66. [CrossRef]
58. Liu, X.; Huang, D.; Lai, C.; Qin, L.; Zeng, G.; Xu, P.; Li, B.; Yi, H.; Zhang, M. Peroxidase-Like Activity of Smart Nanomaterials and Their Advanced Application in Colorimetric Glucose Biosensors. *Small* **2019**, *15*, 1900133. [CrossRef]
59. Sugawa, K.; Tahara, H.; Yamashita, A.; Otsuki, J.; Sagara, T.; Harumoto, T.; Yanagida, S. Refractive Index Susceptibility of the Plasmonic Palladium Nanoparticle: Potential as the Third Plasmonic Sensing Material. *ACS Nano* **2015**, *9*, 1895–1904. [CrossRef]
60. De Marchi, S.; Núñez-Sánchez, S.; Bodelón, G.; Pérez-Juste, J.; Pastoriza-Santos, I. Pd nanoparticles as a plasmonic material: Synthesis, optical properties and applications. *Nanoscale* **2020**, *12*, 23424–23443. [CrossRef]

61. Langhammer, C.; Yuan, Z.; Zoric, I.; Kasemo, B. Plasmonic Properties of Supported Pt and Pd Nanostructures. *Nano Lett.* **2006**, *6*, 833–838. [CrossRef]
62. Rastogi, L.; Dash, K.; Sashidhar, R.B. Selective and sensitive detection of cholesterol using intrinsic peroxidase-like activity of biogenic palladium nanoparticles. *Curr. Res. Biotechnol.* **2021**, *3*, 42–48. [CrossRef]
63. Jin, L.; Meng, Z.; Zhang, Y.; Cai, S.; Zhang, Z.; Li, C.; Shang, L.; Shen, Y. Ultrasmall Pt Nanoclusters as Robust Peroxidase Mimics for Colorimetric Detection of Glucose in Human Serum. *ACS Appl. Mater. Interfaces* **2017**, *9*, 10027–10033. [CrossRef]
64. Gu, S.; Risse, S.; Lu, Y.; Ballauff, M. Mechanism of the Oxidation of 3,3′,5,5′-Tetramethylbenzidine Catalyzed by Peroxidase-Like Pt Nanoparticles Immobilized in Spherical Polyelectrolyte Brushes: A Kinetic Study. *ChemPhysChem* **2020**, *21*, 450–458. [CrossRef] [PubMed]
65. Wunder, S.; Polzer, F.; Lu, Y.; Mei, Y.; Ballauff, M. Kinetic Analysis of Catalytic Reduction of 4-Nitrophenol by Metallic Nanoparticles Immobilized in Spherical Polyelectrolyte Brushes. *J. Phys. Chem. C* **2010**, *114*, 8814–8820. [CrossRef]
66. Abnous, K.; Danesh, N.M.; Ramezani, M.; Taghdisi, S.M.; Emrani, A.S. A novel colorimetric aptasensor for ultrasensitive detection of cocaine based on the formation of three-way junction pockets on the surfaces of gold nanoparticles. *Anal. Chim. Acta* **2018**, *1020*, 110–115. [CrossRef] [PubMed]
67. Bernardi, M.; Palummo, M.; Grossman, J.C. Extraordinary Sunlight Absorption and One Nanometer Thick Photovoltaics Using Two-Dimensional Monolayer Materials. *Nano Lett.* **2013**, *13*, 3664–3670. [CrossRef] [PubMed]
68. Jiang, R.B.; Li, B.X.; Fang, C.H.; Wang, J.F. Metal/semiconductor hybrid nanostructures for plasmon-enhanced applications. *Adv. Mater.* **2014**, *26*, 5274–5309. [CrossRef]
69. Zhou, J.; Yang, T.; Chen, J.; Wang, C.; Zhang, H.; Shao, Y. Two-dimensional nanomaterial-based plasmonic sensing applications: Advances and challenges. *Coord. Chem. Rev.* **2020**, *410*, 213218. [CrossRef]
70. Lee, H.; Park, J.H.; Raza, F.; Yim, D.; Jeon, S.; Kim, H.; Bong, K.W.; Kim, J. Photoactive WS2 Nanosheets Bearing Plasmonic Nanoparticles for Visible Light-Driven Reduction of Nitrophenol. *Chem. Commun.* **2016**, *52*, 6150–6153. [CrossRef]
71. Tseng, W.-B.; Lee, C.-H.; Tseng, W.-L. Poly(diallydimethylammonium chloride)-induced dispersion and exfoliation of tungsten disulfide for the sensing of glutathione and catalytic hydrogenation of p-nitrophenol . *ACS Appli. Nano Mat.* **2018**, *1*, 6808–6817. [CrossRef]
72. Wu, J.; Lu, Y.; Wu, Z.; Li, S.; Zhang, Q.; Chen, Z.; Jiang, J.; Lin, S.; Zhu, L.; Li, C.; et al. Two-dimensional molybdenum disulfide (MoS2) with gold nanoparticles for biosensing of explosives by optical spectroscopy. *Sens. Actuators B* **2018**, *261*, 279–287. [CrossRef]
73. Nirala, N.R.; Pandey, S.; Bansal, A.; Singh, V.K.; Mukherjee, B.; Saxena, P.S.; Srivastava, A. Different shades of cholesterol: Gold nanoparticles supported on MoS2 nanoribbons for enhanced colorimetric sensing of free cholesterol. *Biosens. Bioelectron.* **2015**, *74*, 207–213. [CrossRef]
74. Xu, Y.; Schoonen, M.A. The absolute energy positions of conduction and valence bands of selected semiconducting minerals. *Amer. Miner.* **2000**, *85*, 543–556. [CrossRef]
75. Ma, C.; Ma, Y.; Sun, Y.; Lu, Y.; Tian, E.; Lan, J.; Li, J.; Ye, W.; Zhang, H. Colorimetric determination of Hg2+ in environmental water based on the Hg2+-stimulated peroxidase mimetic activity of MoS2-Au composites. *J. Colloid Interface Sci.* **2019**, *537*, 554–561. [CrossRef]
76. Tao, Z.; Wei, L.; Wu, S.; Duan, N.; Li, X.; Wang, Z. A colorimetric aptamer-based method for detection of cadmium using the enhanced peroxidase-like activity of Au–MoS2 nanocomposites. *Anal. Biochem.* **2020**, *608*, 113844. [CrossRef]
77. Su, S.; Li, J.; Yao, Y.; Sun, Q.; Zhao, Q.; Wang, F.; Li, Q.; Liu, X.; Wang, L. Colorimetric Analysis of Carcinoembryonic Antigen Using Highly Catalytic Gold Nanoparticles-Decorated MoS2 Nanocomposites. *ACS Appl. Bio Mater.* **2019**, *2*, 292–298. [CrossRef] [PubMed]
78. Qu, X.; Zhang, H.; Chen, H.; Aldalbahi, A.; Li, L.; Tian, Y.; Weitz, D.A.; Pei, H. Convection-Driven Pull-Down Assays in Nanoliter Droplets Using Scaffolded Aptamers. *Anal. Chem.* **2017**, *89*, 3468–3473. [CrossRef] [PubMed]
79. Chen, P.; Pan, D.; Fan, C.; Chen, J.; Huang, K.; Wang, D.; Zhang, H.; Li, Y.; Feng, G.; Liang, P.; et al. Gold Nanoparticles for High-throughput Genotyping of Long-range Haplotypes. *Nat. Nanotechnol.* **2011**, *6*, 639–644. [CrossRef]
80. Qu, X.; Wang, S.; Ge, Z.; Wang, J.; Yao, G.; Li, J.; Zuo, X.; Shi, J.; Song, S.; Wang, L.; et al. Programming Cell Adhesion for On-Chip Sequential Boolean Logic Functions. *J. Am. Chem. Soc.* **2017**, *139*, 10176–10179. [CrossRef]
81. Civas, M.; Cetinkaya, O.; Kuscu, M.; Akan, O.B. Biosensor nanoengineering: Design, opera-tion, and implementation for biomolecular analysis. *Sens. Int.* **2020**, *1*, 100040.
82. Wei, Q.; Qi, H.; Luo, W.; Tseng, D.; Ki, S.J.; Wan, Z.; Göröcs, Z.; Bentolila, L.A.; Wu, T.-T.; Sun, R.; et al. Fluorescent Imaging of Single Nanoparticles and Viruses on a Smart Phone. *ACS Nano* **2013**, *7*, 9147–9155. [CrossRef]
83. Smith, Z.J.; Chu, K.; Espenson, A.R.; Rahimzadeh, M.; Gryshuk, A.; Molinaro, M.; Dwyre, D.M.; Lane, S.; Matthews, D.; Wachsmann-Hogiu, S. Cell-Phone-Based Platform for Biomedical Device Development and Education Applications. *PLoS ONE* **2011**, *6*, e17150. [CrossRef]
84. Wang, Y.; Liu, X.; Chen, P.; Tran, N.T.; Zhang, J.; Chia, W.S.; Boujday, S.; Liedberg, B. Smartphone spectrometer for colorimetric biosensing. *Analyst* **2016**, *141*, 3233–3238. [CrossRef] [PubMed]
85. Fantoni, A.; Vygranenko, Y.; Maçarico, A.; Serafinelli, C.; Fernandes, M.; Mansour, R.; Jesus, R.; Vieira, M. Arrayed graphene enhanced surface plasmon resonance for sensing applications. In Proceedings of the Optical Components and Materials XVIII, SPIE OPTO, Online, 6–12 March 2021; SPIE: Bellingham, WA, USA, 2021; Volume 11682, p. 1168213.